UDC 519.711, 621.923.6 **doi: 10.20998/2078-7405.2026.104.06**

THE EFFECT OF MECHANICAL AND GEOMETRIC CHARACTERISTICS OF INHOMOGENEOUS REGIONS ON THE INTENSITY OF CRACK FORMATION DURING THE GRINDING OF PARTS MADE OF FUNCTIONALLY-GRADIENT MATERIALS

Anatoliy **Usov** [0000-0002-3965-7611], Maksym **Kunitsyn** [0000-0003-1764-8922], Yuliia **Sikirash** [0000-0003-0853-582X], Valeriy **Davydiuk** [0000-0002-9460-9129]

National University "Odessa Polytechnic", Odessa, Ukraine
m.v.kunitsyn@op.edu.ua

Received: 02 April 2026/ Revised: 18 April 2026/ Accepted: 28 April 2026 / Published: 15 May 2026

Abstract. *The lack of research on the specifics of the initiation of grinding cracks and their development into main cracks depending on the design, technological, and structural inhomogeneities of the material of the products does not allow for the unambiguous application of existing recommendations for eliminating the defects in question. This work is devoted to investigating the influence of inherent inhomogeneities in the surface layer, their geometry, and mechanical characteristics in products made of functionally graded materials on the selection of technological conditions for defect-free machining of parts. It has been established that the magnitude of the stress intensity factors for inherent inhomogeneities formed in the surface layer of products made of functionally graded materials is influenced by the size and orientation of these defects, their depth of occurrence and mutual arrangement, and the magnitude of the heat flux during grinding. The geometry and properties of inclusions formed by previous operations in the surface layer can create conditions for both the inhibition and the development of grinding cracks. If the heat flux is directed parallel to the inclusion axis and a straight, thermally isolated crack, then when the linear thermal expansion coefficient of the inclusion is greater than that of the matrix, an increase in the stiffness of the inclusion leads to an increase in the stress intensity factors K_I ($K_{II} = 0$) for various ratios of the thermal conductivity coefficients of the material components. This leads to the propagation of microcracks. Conversely, if the thermal expansion coefficient of the inclusion is lower than that of the matrix, a decrease in the stiffness of the inclusion leads to a decrease in the stress intensity factors K_I ($K_{II} = 0$) for the same ratios of thermal conductivity coefficients, i.e., conditions favorable for the non-propagation of microcracks are present. Therefore, when determining defect-free grinding parameters, it is necessary, first and foremost, to establish the maximum permissible cutting depths. In doing so, it is also important to have information not only on the thermophysical and mechanical properties of the material and the presence of inhomogeneities in the surface layer, but also on its processing conditions.*

Keywords: *functionally graded materials; inhomogeneities; grinding; crack formation.*

1. Introduction

Establishing relationships between the most important operational properties

of parts (wear resistance, fatigue and long-term strength, contact stiffness, magnetic properties, etc.) and the technological parameters of grinding—the micro-relief of the machined surface, microhardness, the presence of microcracks and chips, and the depth of the hardened layer—is one of the most important tasks in mechanical engineering technology.

The works [1], [2] are devoted to the study of thermophysical phenomena accompanying the finishing operation and determining the quality of the surface layer of products made of functionally graded materials, as well as to establishing their influence on crack and burn formation based on a quantitative analysis of the thermal stress state.

However, the problem of ensuring the required quality of the working surface of products made of functionally graded materials during finishing operations cannot be solved by thermal criteria alone. Given that the materials used to manufacture parts exhibit a high degree of heterogeneity, significant changes in the distribution of temperatures and deformations should be expected in areas where heterogeneities accumulate, as well as in their geometry; this, in turn, can lead to the formation of local deformations and the appearance of cracks on the working surfaces of ground products.

2. Analysis of sources and problem description

Stresses in workpieces during grinding typically propagate through a very thin layer several hundredths of a millimeter thick. The counteracting compensating stresses, on the other hand, are distributed over a significantly larger volume but have a negligible absolute magnitude, so their influence on the part's operational properties can be disregarded. Maximum stresses thus occur near the machined surface, at a shallow depth.

A number of studies [3] have proposed a method for calculating the maximum thermoelastic stresses functionally related to the processing conditions. The resulting relationships were used as criteria for defect-free processing based on the absence of crack formation.

In cases where the workpieces being processed are homogeneous pieces (coated workpieces), their stress-strain state depends on the properties of their constituent materials. Taking into account their physical and mechanical properties, as well as the coating thickness, allowed the author of [4], [5] to determine, based on the solution to the problem [6], the stress state resulting from grinding temperatures at the coating-matrix interface and to develop limit defect-free grinding cycles for coated parts.

The studies of the causes of grinding cracks presented in the works [7], [8] from the perspective of structural and phase transformations that generate corresponding structural stresses— $\sigma_{\text{str}}(M, \tau)$ —are also of a specific nature and do not allow for

a comprehensive understanding of the true picture of crack-type defect formation on the machined surface. The fact is that both structural and phase transformations (in volumes sufficient to generate destructive structural stresses) must occur at relatively low rates of heating (or cooling) and over a significant period of time. Meanwhile, grinding is characterized by short durations, high heating rates of the order of 3,000–50,000 °C/s, and approximately the same cooling rates [9]. These, in turn, are conditions close to thermal shock [10], [11], during which thermal stresses reach very high values.

The known functional relationships between process parameters and grinding temperature [2], [12] make it possible, using appropriate techniques, to eliminate burn marks on the machined surfaces of products made from functionally graded materials that do not contain design- or process-related inhomogeneities and whose material does not contain significant inhomogeneities. Studies of the conditions for improving the quality of machined surfaces by eliminating defects such as cracks were conducted primarily at the level of identifying qualitative relationships between process parameters and the physical and mechanical properties of the materials being ground [13]. The quantitative relationships between stresses and processing conditions obtained in a number of studies [14] are of a specific nature and do not reflect the general patterns of the stress-strain state of the surface layer depending on technological conditions and the properties of the materials being processed. In later studies [15], [16], the stress state of ground surfaces was evaluated using numerical methods.

However, the lack of studies on the specifics of the initiation of grinding cracks and their development into main cracks depending on the design, technological, and structural inhomogeneities of the material of the products does not allow for the unambiguous application of existing recommendations for eliminating the defects in question.

3. Research objectives

Therefore, the objective of this work is to investigate the influence of inherent inhomogeneities in the surface layer, their geometry, and mechanical characteristics in products made of functionally graded materials on the selection of technological conditions for defect-free machining of parts.

This objective can be achieved by solving the following tasks:

1. Create a mathematical model describing the thermomechanical processes in the surface layer during the grinding of products made of functionally graded materials, taking into account the inhomogeneities and their geometry formed during previous operations, starting from the production of the blank.

2. Select criteria for crack and burn formation on the machined surfaces and establish their relationship with the investigated technological parameters of the grinding process.

3. Develop the prerequisites for optimizing the thermomechanical state of the surface layer of products made of functionally graded materials during the grinding process, thereby preventing the occurrence of grinding defects such as cracks and burn marks.

4. Determine the technological capabilities for controlling the quality of the surface layer of parts using the established relationships between the physical and mechanical properties of functionally graded materials, the inhomogeneities and their geometry within the machined layer, and the technological parameters of the grinding process.

4. Research methods

The grinding process of machine parts is accompanied by both thermal and mechanical phenomena, which, interacting with each other, determine the quality of the surface layer. A quantitative description of these phenomena requires the selection of specific models. Due to the interconnection and interdependence of phenomena and processes during metal grinding, it becomes evident that the stress-strain state of the surface layer is determined primarily by the grinding temperature. If we use a thermoelastic body model that reflects the interrelationship between mechanical and thermal phenomena under finite heat fluxes, we can make significant progress in research on the influence of thermomechanical phenomena accompanying the grinding process on the quality characteristics of the machined surfaces of parts

For further studies of the kinetics of thermomechanical processes, we will use the following system of differential equations [17] as the main theoretical framework, which describes the interaction between the strain field and the temperature field:

$$\begin{gathered} G\Delta\vec{U}_j + (\lambda_t + G)\ grad\ div\ \vec{U}_j - \rho\frac{\partial^2\vec{U}_j}{\partial\tau^2} + P_j = \alpha_t\beta_t\ grad\ T \\ \Delta T - \frac{1}{a}\frac{\partial T}{\partial\tau} - \eta l\frac{\partial}{\partial\tau}\ div\ \vec{U}_j = -\frac{W}{\lambda} + C_q^{-2}\frac{\partial^2 T}{\partial t^2} \end{gathered} \quad (1)$$

where λ_t, G are Lamé constants; $\beta_t = 3\lambda_t + 2G$; ρ is the density of the processed material; α_t is the thermal coefficient of linear expansion of the metal; $a = \lambda/C_v$ is the thermal conductivity; λ is the thermal conductivity; C_v is the specific heat capacity; $\vec{U}(\Phi, t)$ is the total displacement vector of the internal point $\Phi\ (x, y, z)$ of the surface layer under the action of thermomechanical phenomena accompanying the grinding process: $l = 1 + \tau r\ \delta/\delta$ (τ is the relaxation time); $\eta =$

$\alpha t \beta t T(\Phi, \tau) \,/\, \lambda$; W is the power of the heat source; C_q is the heat diffusion coefficient in the workpiece material; τ is the time; P_j are cutting forces;

$$grad\, T(x,y,z) = \frac{\partial T}{\partial x}\vec{\imath} + \frac{\partial T}{\partial y}\vec{\jmath} + \frac{\partial T}{\partial z}\vec{k}$$

$$div\, \vec{U}_j = \frac{\partial U}{\partial x} + \frac{\partial U_y}{\partial y} + \frac{\partial U_z}{\partial z}, \qquad j \rightleftarrows x, y, z$$

Since thermal phenomena prevail over mechanical forces during grinding, the term accounting for the conversion of mechanical energy into heat can be neglected in the heat conduction equation, and we arrive at a parabolic-type heat conduction equation. To solve the given system (1) in explicit form, we will neglect the influence of inertial terms and the finiteness of the heat propagation speed. Furthermore, to overcome the analytical difficulties associated with solving spatial thermoelasticity problems, we will consider a plane problem. This transition is justified by the fact that, for investigating the thermomechanical state of ground surfaces, information regarding the propagation of temperatures and deformations with depth and in the direction of the tool's movement is crucial.

An analysis of large-scale interaction schemes between the wheel and the workpiece surface has shown [18], [19] that the curvature of the wheel and the workpiece within the contact zone has a negligible effect on the geometric interaction scheme between the wheel and the workpiece. Therefore, when formulating the computational model, we assume that the workpiece is a half-plane whose surface layer contains inhomogeneities of inherent origin. This allows us to study thermomechanical processes during the grinding of workpieces with inhomogeneities Δa_K having different geometries and locations within the matrix—the material of the workpiece. This scheme determines the thermal and deformation coupling conditions at their boundaries - a_K.

We will account for the influence of structural inhomogeneities in the machined surface in the model by the presence of inclusions and defects such as cracks.

The equation of transient heat conduction:

$$\frac{\partial T}{\partial \tau} = a^2\left(\frac{\partial^2 T}{\partial x^2} + \frac{\partial^2 T}{\partial y^2}\right) \tag{2}$$

b) Lame's elasticity equations in displacements:

$$\begin{aligned} &\frac{\partial \theta}{\partial x}\cdot\frac{1}{1-2\mu} + \Delta\vec{U} = b^T\frac{\partial T}{\partial x}, \qquad \vec{U} = \frac{U}{2G}, \qquad \vec{\mathrm{V}} = \frac{\mathrm{V}}{2\mathrm{G}}; \\ &\frac{\partial \theta}{\partial y}\cdot\frac{1}{1-2\mu} + \Delta\vec{U} = b^T\frac{\partial T}{\partial y}, \qquad b^T = \frac{4G(1+\mu)}{1-2\mu}\alpha t \end{aligned} \tag{3}$$

c) Initial conditions:

$$T(x,y,o) \;=\; 0 \tag{4}$$

d) boundary conditions for the temperature and strain fields:

$$\frac{\partial T}{\partial x} = -\frac{q(y,t)}{\lambda}, \qquad |y| < a, \qquad -\frac{\partial T}{\partial x} + jT = 0, \qquad |y| > a;$$
$$(\sigma_x(x,y,t)|_{x=0} = \tau_{xy}((x,y,t)\big|_{x=0} = 0 \tag{5}$$

e) Coupling conditions between the boundaries of the inhomogeneities and the base material:

for temperature fields	for strain fields
$\overset{k-1}{T}(a_k - 0, y, \tau) = \overset{k}{T}(a_k + 0, y, \tau)$	$\overset{k-1}{V_j}(a_k - 0, y) = \overset{k}{V_j}(a_k + 0, y)$
$\lambda_{k-1}\frac{\partial \overset{k-1}{T}}{\partial x}(a_k - 0, y, \tau) = \lambda_k \frac{\partial \overset{k}{T}}{\partial x}(a_k + 0, y, \tau)$	$\overset{k-1}{\sigma}_x(a_k - 0, y) = \overset{k}{\sigma_x}(a_k + 0, y)\ \overset{k-1}{\tau}_{xy}(a_k - 0, y) = \overset{k}{\tau_{xy}}(a_k + 0, y)$

(6)

e) Discontinuity conditions of the solution:

at inclusions:	at crack-like defects:
$< \tilde{u} >= 0, \quad < \sigma_x > \neq 0$	$< \sigma_x >= 0, \quad < \tilde{u} > \neq 0$
$< v >= 0, \quad < \tau_{xy} > \neq 0$	$< \tau_{xy} >= 0, \quad < \tilde{v} > \neq 0$

The conditions for the discontinuity of solution (6) at inhomogeneities such as inclusions and crack-like defects should be understood as follows [2], [20]:

$$< \tilde{u} \geq \tilde{u}(-0, y) - \tilde{u}(+0, y), \qquad < \sigma_x \geq \sigma_x(-0, y) - \sigma_x(+0, y)$$
$$< v >= \hat{v}(-0, y) - \hat{v}(+0, y), \qquad < \tau_{xy} >= \tau_{xy}(-0, y) - \tau_{xy}(+0, y)$$

5. Research results

The presence of stress concentrators in the surface layer of ground products—which include various types of defects introduced during the production of the blank and subsequent processing steps—significantly complicates the investigation of the causes of crack formation. Therefore, when determining the limit equilibrium state of the deformable surface layer, the values of the stress and strain components at the tip of the stress concentrator must be substituted into the classical strength criteria. This approach is used in fracture mechanics [21], where new strength criteria are formulated as specific invariants, both in models of continuum mechanics and in models that account for micro-inhomogeneities in the material being processed. Of the criteria available in fracture mechanics, which are divided into energy, force, and deformation criteria [22], [23], the most suitable for our case are the force-based criteria associated with the use of the stress intensity factor (SIF) [23], [24]. In the most general case, the distribution of strains in the vicinity of the crack-like defect is represented as a superposition of three partial strains corresponding to the three main types of crack surface displacement: normal separation, transverse, and longitudinal shear.

The stress intensity factors K_I, K_{II}, and K_{III} serve as a measure of stress singularity near the tip of a crack-like defect. The critical stress intensity, K_C, is a material property. When loading causes the stress intensity to reach the critical value,

the crack-like defect transforms into a main crack. The critical stress is inversely proportional to the square root of the initial length of the crack-like defect [25]:

$$\sigma_C = \frac{K_{1C}}{\sqrt{\pi l}}$$

where $2l$ is the initial length of the crack-like defect, and the subscript 1 denotes the first type of fracture.

The thermally stressed grinding process generates thermomechanical stresses in the surface layer, which, in the presence of inhomogeneous defects, can lead to their propagation in the form of chips and a network of cracks even in the absence of external mechanical loads.

Let there be defects in an elastic half-plane on the lines a_1, a_2, ..., a_k has $|\tilde{y}_1| < l_1$, $|\tilde{y}_2| < l_2, \ldots, |\tilde{y}_K| < l_K$, across which the displacement and stress fields undergo discontinuities. Hereinafter, we will consider a system of defects consisting of two cracks ($k = 1, 2$) located in local coordinates at $\tilde{x}_1 o_1 \tilde{y}_1$ ($k = 1$) and $\tilde{x}_2 o_2 \tilde{y}_2$ ($k = 2$), respectively. Fig. 1 shows a computational scheme for determining the influence of defects on crack initiation under thermal loading.

Let us consider the jumps in displacements and stresses at the defects:

$$\langle \tilde{V}_k(\tilde{y}) \rangle = \tilde{V}_k(-0, \tilde{y}) - \tilde{V}_k(+0, \tilde{y}), \qquad \left\langle \overset{k}{\sigma}_x(\tilde{y}) \right\rangle = \overset{k}{\sigma}_x(-0, \tilde{y}) - \overset{k}{\sigma}_x(+0, \tilde{y})$$

$$\langle \tilde{U}_k(\tilde{y}) \rangle = \tilde{U}_k(-0, \tilde{y}) - \tilde{U}_k(+0, \tilde{y}), \qquad \left\langle \overset{k}{\tau}_{xy}(\tilde{y}) \right\rangle = \overset{k}{\tau}_{xy}(-0, \tilde{y}) - \overset{k}{\tau}_{xy}(+0, \tilde{y})$$

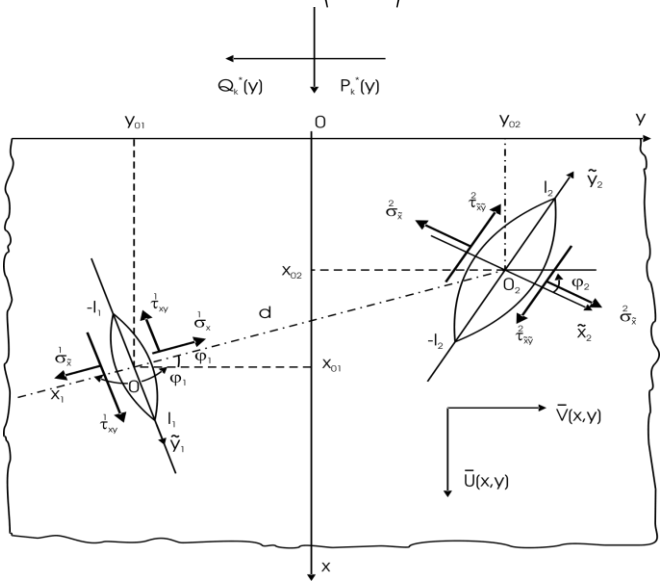

Fig. 1. Calculation scheme for determining the influence of defects on the intensity of crack formation under thermal loading.

According to conditions (6), at crack-type defects, the jumps in normal and tangential stresses are zero, i.e., $< \overset{K}{\sigma_r}(y) \geq 0$, $< \overset{K}{T_{xy}}(y) \geq 0$. The displacements $\widetilde{U}_K(\tilde{x},\tilde{y})$, $V_K(\tilde{x},\tilde{y})$, $\theta_K(\tilde{x},\tilde{y})$ must satisfy the Lamé equations:

$$\frac{\tilde{\Theta}'}{1-2\mu} + \Delta\widetilde{U}_k = b^T T', \qquad \frac{\tilde{\Theta}`}{1-2\mu} + \Delta\tilde{V}_k = b^T T`, \qquad \tilde{\Theta}_k = \widetilde{U}_k^{'} + \tilde{V}`_k, \quad b^T = \frac{4G(1+\mu)dt}{1-2\mu}$$

Using Treffz's representations [2], [26], [27] in the Fourier transformants with respect to the variable y, one can determine the displacements $\widetilde{U}_{\beta K}(\tilde{x})$, $\tilde{V}_{\beta K}(\tilde{x})$ and the stresses $\overset{k}{\sigma}_{\tilde{x}\beta}(\tilde{x})\overset{k}{\tau}_{\tilde{x}\beta}(\tilde{x})$, $\overset{k}{\sigma}_{\tilde{x}\beta}(\tilde{x}) = \overset{k}{\sigma}_{y\beta}(\tilde{x})\tilde{y}$.

Returning to the original discontinuous solutions for the stress in local coordinates $\tilde{x}_K o_K \tilde{\tilde{y}}_K$, via the derivatives of the displacement jumps $< \widetilde{U}_K^{'}(\tilde{y}) >$, $< V_K^{'}(\tilde{y}) >$ are expressed as:

$$\overset{k}{\sigma}{}^{I}_{\tilde{x}}(\tilde{x},\tilde{y}) = \frac{1}{4\pi(1-\mu)} \int_{-e_k}^{e_k} \langle \widetilde{U}_k^{'}(r)\rangle \frac{(\tilde{y}-r)[(4\mu-3)(((\tilde{y}-r)^2+\tilde{x}^2)-\tilde{x}^2]}{[(\tilde{y}-r)^2+\tilde{x}^2]^2}\, dr - \\ - \frac{\tilde{x}}{4\pi(1-\mu)} \int_{-e_k}^{e_k} \langle \tilde{V}_k^{'}(r)\rangle \frac{((\tilde{y}-r)^2-\tilde{x}^2)}{[(\tilde{y}-r)^2+\tilde{x}^2]^2} dr \tag{7}$$

$$\overset{k}{\tau}{}^{I}_{\tilde{x}}(\tilde{x},\tilde{y}) = \frac{-\tilde{x}}{4\pi(1-\mu)} \int_{-e_k}^{e_2} \langle \widetilde{U_k^{'}}(r)\rangle \frac{\left((\tilde{y}-r)^2-\widetilde{x^2}\right)}{\left[(\tilde{y}-r)^2+\widetilde{x^2}\right]^2} dr \\ - \frac{1}{4\pi(1-\mu)} \int_{-e_k}^{e_2} \langle \widetilde{V_k^{'}}(r)\rangle \frac{(\tilde{y}-r)^2}{\left[(\tilde{y}-r)^2+\widetilde{x^2}\right]^2} dr \tag{8}$$

$$\overset{k'}{\sigma}_y(\tilde{x},\tilde{y}) = \int_{-e_k}^{e_k} \langle \widetilde{U}_k^{'}(r)\rangle \left\{ \frac{(\tilde{y}-r)}{4\pi[(\tilde{y}-r)^2+\tilde{x}^2]^2} \left(1 + \frac{\tilde{x}^2}{(1-\mu)[(\tilde{y}-r)^2+\tilde{x}^2]^2}\right)\right\} dr + \\ + \frac{1}{2\pi(1-\mu)} \int_{-e_k}^{e_k} \langle \tilde{V}_k^{'}(r)\rangle \left\{ (1+\mu)\tilde{x} l_n[(\tilde{y}-r)^2+\tilde{x}^2] + \frac{\tilde{x}[\tilde{x}^2+(\tilde{y}-r)^2]^2}{2[\tilde{x}^2+(\tilde{y}-r)^2]^2}\right\} dr \tag{9}$$

We find the compensating stresses as follows. We express the discontinuous solutions (7) – (9) in global coordinates and, setting $x = 0$, find the stresses at the boundary.

They will be equal to:

$$\overset{k}{\sigma}{}^{I}_{x}(0,y) = \int_{-e_k}^{e_k} \left[\langle \widetilde{U}_k^{'}(r)\rangle \overset{k}{R}_1(y,r) + \langle \tilde{V}_k^{'}(r)\rangle \overset{k}{N}_1(y,r)\right] dr = P_k^*(y) \tag{10}$$

$$\overset{k}{\tau}_{xy}(0,y) = \int_{-e_k}^{e_k} \left[\langle \widetilde{U}_k^{'}(r)\rangle \overset{k}{R}_2(y,r) + \langle \tilde{V}_k^{'}(r)\rangle \overset{k}{N}_2(y,r)\right] dr = q_k^*(y) \tag{11}$$

Here, $\overset{K}{R}_j(x,y)$, $\overset{K}{N}_j(y,z)$ are the kernels ($k = 1,2$); characterizing the coordinate transformation (local $\tilde{x}_K o_K \tilde{y}_K$ to global XOY and the expressions of stress components in global coordinates. Taking as boundary conditions ($x = 0$):

$$\sum_{k=1}^{2} \overset{k}{\sigma}_x(0,y) = -P_k^*(y) = \sigma_x(0,y) \tag{12}$$

$$\sum_{k=1}^{2} \overset{k}{\tau}_{xy}(0,y) = -q_k^*(y) = \tau_{xy}(0,y) \tag{13}$$

we find the stress state of the surface layer:

$$\begin{aligned}\sigma_y^{II}(x,y) = {} & \frac{-\alpha_1 x\mu^*}{\pi}\sum_{k=1}^{2}\int_{-e_k}^{e_k}\left[\langle\tilde{U}_k'(r)\rangle\overset{k}{R}_1(y,r) + \langle\tilde{V}_k'(r)\rangle\overset{k}{N}_1(y,r)\right]\frac{dr}{x^2+(y-r)^2} + \\ & + \frac{\alpha_2 x}{\pi}\sum_{k=1}^{2}\int_{-e_k}^{e_k}\left[\langle\tilde{U}_k'(r)\rangle\overset{k}{R}_1(y,r) + \langle\tilde{V}_k'(r)\rangle\overset{k}{N}_1(y,r)\right]\frac{[x^2+(y-r)^2]dr}{[x^2+(y-r)^2]^2} + \\ & + \frac{\alpha_3+\mu^*}{2\pi}\sum_{k=1}^{2}\int_{-e_k}^{e_k}\left[\langle\tilde{U}_k'(r)\rangle\overset{k}{R}_1(y,r) + \langle\tilde{V}_k'(r)\rangle\overset{k}{N}_1(y,r)\right]\frac{(y-r)dr}{x^2+(y-r)^2} - \\ & - \frac{2\alpha_4 x}{\pi}\sum_{k=1}^{2}\int_{-e_k}^{e_k}\left[\langle\tilde{U}_k'(r)\rangle\overset{k}{R}_1(y,r) + \langle\tilde{V}_k'(r)\rangle\overset{k}{N}_1(y,r)\right]\frac{(y-r)dr}{[x^2+(y-r)^2]^2}\end{aligned} \tag{14}$$

$$\begin{aligned}\tau_{xy}^{II}(x,y) = {} & \frac{1}{2\pi}\left(\nu + \frac{\tilde{\mu}_1^*}{1-\mu}\right)\sum_{k=1}^{2}\int_{-e_k}^{e_k}\left[\langle\tilde{U}_k'(r)\rangle\overset{k}{R}_1(y,r) + \langle\tilde{V}_k'(r)\rangle\overset{k}{N}_1(y,r)\right]\frac{(y-r)dr}{x^2+(y-r)^2} \\ & + \\ & + \frac{-x\tilde{\mu}_1^*}{2\pi(1-\mu)}\sum_{k=1}^{2}\int_{-e_k}^{e_k}\left[\langle\tilde{U}_k'(r)\rangle\overset{k}{R}_1(y,r) + \langle\tilde{V}_k'(r)\rangle\overset{k}{N}_1(y,r)\right]arctg\frac{(y-r)dr}{|x|} - \\ & - \frac{x\nu^*}{2\pi}\sum_{k=1}^{2}\int_{-e_k}^{e_k}\left[\langle\tilde{U}_k'(r)\rangle\overset{k}{R}_1(y,r) + \langle\tilde{V}_k'(r)\rangle\overset{k}{N}_1(y,r)\right]ln\frac{1}{\sqrt{x^2+(y-r)^2}}dr - \\ & - \frac{x^2(1+\nu^*)}{2\pi(1-\mu)}\sum_{k=1}^{2}\int_{-e_k}^{e_k}\left[\langle\tilde{U}_k'(r)\rangle\overset{k}{R}_1(y,r) + \langle\tilde{V}_k'(r)\rangle\overset{k}{N}_1(y,r)\right]\frac{(y-r)dr}{[x^2+(y-r)^2]^2} - \\ & - \frac{x\tilde{\mu}_1^*}{4\pi(1-\mu)}\sum_{k=1}^{2}\int_{-e_k}^{e_k}\left[\langle\tilde{U}_k'(r)\rangle\overset{k}{R}_1(y,r) + \langle\tilde{V}_k'(r)\rangle\overset{k}{N}_1(y,r)\right]\frac{x^2+(y-r)^2}{[x^2+(y-r)^2]^2}dr + \\ & + \frac{x}{4\pi(1-\mu)}\sum_{k=1}^{2}\int_{-e_k}^{e_k}\left[\langle\tilde{U}_k'(r)\rangle\overset{k}{R}_1(y,r) + \langle\tilde{V}_k'(r)\rangle\overset{k}{N}_1(y,r)\right]\frac{(y-r)(3x^2+(y-r)^2)}{[x^2+(y-r)^2]^3}dr - \\ & + \frac{x}{4\pi(1-\mu)}\sum_{k=1}^{2}\int_{-e_k}^{e_k}\left[\langle\tilde{U}_k'(r)\rangle\overset{k}{R}_1(y,r) + \langle\tilde{V}_k'(r)\rangle\overset{k}{N}_1(y,r)\right]\frac{(y-r)(3x^2+(y-r)^2)}{[x^2+(y-r)^2]^3}dr -\end{aligned} \tag{15}$$

$$-\frac{x(1+\nu^*)}{\pi}\sum_{k=1}^{2}\int_{-e_k}^{e_k}\left[\left\langle\tilde{U}_k'(r)\right\rangle\overset{k}{R}_1(y,r)+\left\langle\tilde{V}_k'(r)\right\rangle\overset{k}{N}_1(y,r)\right]\frac{dr}{x^2+(y-r)^2}$$

$$\sigma_x^{II}(x,y)=\gamma_1\sum_{k=1}^{2}\int_{-e_k}^{e_k}\left[\left\langle\tilde{U}_k'(r)\right\rangle\overset{k}{R}_1(y,r)+\left\langle\tilde{V}_k'(r)\right\rangle\overset{k}{N}_1(y,r)\right]\frac{2xdr}{x^2+(y-r)^2}-$$
$$-x\gamma_2\sum_{k=1}^{2}\int_{-e_k}^{e_k}\left[\left\langle\tilde{U}_k'(r)\right\rangle\overset{k}{R}_1(y,r)+\left\langle\tilde{V}_k'(r)\right\rangle\overset{k}{N}_1(y,r)\right]\frac{2[x^2+(y-r)^2]dr}{[x^2+(y-r)^2]^2}+$$
$$+2\gamma_3\sum_{k=1}^{2}\int_{-e_k}^{e_k}\left[\left\langle\tilde{U}_k'(r)\right\rangle\overset{k}{R}_1(y,r)+\left\langle\tilde{V}_k'(r)\right\rangle\overset{k}{N}_1(y,r)\right]\frac{(y-r)dr}{x^2+(y-r)^2}- \quad (16)$$
$$-4x^2\gamma_4\sum_{k=1}^{2}\int_{-e_k}^{e_k}\left[\left\langle\tilde{U}_k'(r)\right\rangle\overset{k}{R}_1(y,r)+\left\langle\tilde{V}_k'(r)\right\rangle\overset{k}{N}_1(y,r)\right]\frac{(y-r)dr}{[x^2+(y-r)^2]^2}$$

In equations (14) – (16), the following notation is used:

$$\bar{\mu}_1^*=\frac{(3-4\mu)(1-2\mu)}{4\mu(1-2\mu)},\bar{\mu}_2^*=\frac{3-4\mu}{2\mu};\nu=\frac{1-2\mu}{2(1-2\mu)};\nu^*=\frac{3-4\mu}{4\mu(1-2\mu)}$$

$$\mu_1^*=\frac{1-2\mu}{2(1-\mu)}\bar{\mu}_1^*;\quad \mu_2^*=\frac{1-2\mu}{2(1-\mu)}\bar{\mu}_2^*;\quad \mu^*=\frac{1}{4\pi(1-\mu)}$$

$$\alpha_1=\frac{1+\bar{\mu}_2^*+\mu_2^*}{2};\quad \alpha_2=\frac{\mu_1^*-1-\bar{\mu}_2^*}{4\pi(1-\mu)};\quad \alpha_3=\mu_1^*+\nu;\quad \alpha_4=\frac{\mu_2^*-\bar{\mu}_1^*+1}{4\pi(1-\mu)}$$

$$\gamma_1=\frac{\mu(\bar{\mu}_1^*-\bar{\mu}_2^*)-(\mu+\bar{\mu}_2^*-2\mu\bar{\mu}_2^*)}{4\pi(1-\mu)};\quad \gamma_2=\frac{\bar{\mu}_1^*-1-\bar{\mu}_2^*}{8\pi(1-\mu)}$$

$$\gamma_3=\frac{2(\mu\bar{\mu}_1^*-\mu\bar{\mu}_2^*-\mu)-(3-4\mu)+(1-2\mu)\bar{\mu}_1^*-2(1-\mu)\bar{\mu}_2^*}{8\pi(1-\mu)};\quad \gamma_4=\frac{\bar{\mu}_1^*-\bar{\mu}_2^*-1}{8\pi(1-\mu)}$$

The thermoelastic stresses generated by the heat flux $q(y,t)$ acting at the boundary $x=0$, in the contact zone $|y|<a$, and by heat transfer according to Newton-Richman's law $\lambda\delta T/\delta x+\gamma T=0$ [28], outside this zone, i.e., $|y|>a$, we obtain from the solution of problem (2)–(6) (the special case $k=0$, $0\le x<\Delta$). In global coordinates, these stresses are expressed as:

$$\sigma_x^{III}(x,y)=\frac{2\alpha_1(x^2-y^2)}{\pi[x^2+y^2]^2}-\frac{2\alpha_2 y(3x^2-y^2)}{\pi[x^2+y^2]^3}+\frac{(\alpha_3-x\alpha_4)}{\pi}\frac{2x(x^2-3y^2)}{[x^2+y^2]^3}-$$
$$-\frac{x\alpha_5}{\pi}\frac{\Gamma(4)\cos\left(\frac{4x}{\sqrt{x^2+y^2}}\right)}{[x^2+y^2]^2}+\frac{b^T}{2\pi}\int_{-\infty}^{\infty}\int_{0}^{\infty}e^{-i\beta y}\left[T_\beta''(\xi)\Phi_\beta(x-\xi)+\right. \quad (17)$$
$$\left.+T_\beta'(\xi)\Phi_\beta'(x-\xi)-\lambda^2\beta^2T_\beta(\xi)\Phi_\beta(x-\xi)\right]d\xi d\beta$$

$$\tau_{xy}^{III}(x,y)=\frac{\gamma_1 2xy}{\pi[x^2+y^2]^2}-\frac{\gamma_2 x(x^2-3y^2)}{\pi[x^2+y^2]^3}+ \quad (18)$$

$$+\frac{\gamma_3}{\pi}\frac{y(3x^2-y^2)}{[x^2+y^2]^3}-\frac{\gamma_4 x}{\pi}\frac{\Gamma(4)\,sin(\frac{4x}{\sqrt{x^2+y^2}})}{[x^2+y^2]^2}-$$
$$-\frac{b^T}{2\pi}\int_{-\infty}^{\infty}\int_{0}^{\infty}e^{-i\beta y}\left[2T_\beta^{'}(\xi)\Phi_\beta(x-\xi)+T_\beta(\xi)\Phi_\beta^{'}(x-\xi)\right]d\xi d\beta$$

$$\sigma_y^{III}(x,y)=\frac{b_1}{\pi}\frac{x^2-y^2}{[x^2+y^2]^2}-\frac{b_2+b_3x}{\pi}\frac{x(x^2-3y^2)}{[x^2+y^2]^3}+$$
$$+\frac{b_4 x\Gamma(4)\,cos(\frac{4x}{\sqrt{x^2+y^2}})}{[x^2+y^2]^2}- \qquad (19)$$
$$-\frac{b^T}{2\pi}\int_{-\infty}^{\infty}\int_{0}^{\infty}\beta^2 e^{-i\beta y}\,T_\beta(\xi)\Phi_\beta(x-\xi)d\xi d\beta$$

Returning to the solutions found for the normal $\sigma_x^{II}(x,y)$, $\sigma_x^{III}(x,y)$, and tangent $\tau_{xy}^{II}(x,y)$, $\tau_{xy}^{III}(x,y)$ stresses in local coordinates and using the obvious conditions:

$$\lim_{\tilde{x}\to 0}\left[\overset{k}{\sigma_{\tilde{x}}^{I}}(\tilde{x},\tilde{y})+\overset{k}{\sigma_x^{II}}(\tilde{x},\tilde{y})+\overset{k}{\sigma_x^{III}}(\tilde{x},\tilde{y})\right]=0$$
$$\lim_{\tilde{x}\to 0}\left[\overset{k}{\tau_{xy}^{I}}(\tilde{x},\tilde{y})+\overset{k}{\tau_{xy}^{II}}(\tilde{x},\tilde{y})+\overset{k}{\tau_{xy}^{III}}(\tilde{x},\tilde{y})\right]=0 \qquad (20)$$

We finally arrive at a system of 4 singular integral equations with respect to the sought-after derivatives of the displacement jumps $<\tilde{U}_K^{'}(y)>,<\tilde{V}_K^{'}(y)>(K=1,2)$ [29], [30]:

Of greatest interest is the behavior of the stresses $\sigma_x(o,y)+iT_{xy}(o,y)$ for $y\to lK\pm o$. These stresses determine the nature of the stress intensity factors—SIFs: K_I and iK_{II}.

Consider the case of a crack-type defect of length $2l$, located in a surface layer of thickness $2h$ and arbitrarily oriented. The stress state of the surface layer is determined by the disturbance near the crack of a given temperature field $T_q(x,y,\tau)$. If the temperature field is described by the function $T_o(x,y,\tau)=q(\tau)(ycos\beta+xsin\beta)$, then to determine the stress intensity factors, we have the formula:

$$K_I^{\pm}-iK_{II}^{\pm}=\mp i\frac{\sqrt{\pi l}Hql}{\lambda}sin(\beta-\phi)\times$$
$$\times\left\{1-\frac{\delta^2}{2}(\alpha_1-N_{11})-\frac{\delta^4}{4}\left[d_2+\frac{3}{2}d_3-d_1N_{11}-N_{11}^2+N_{31}\right]+0(\delta^6)\right\} \qquad (21)$$

where β is the angle between the direction of the heat flux and the Oy axis; ϕ is the angle between the defect axis and the Ox axis; $\delta=l/h$ is the dimensionless width of the band:

$$d_1=-\left(i\,sin\,2\,\phi+e^{-4i\phi}\right)I_1-\frac{1}{2}e^{-2i\phi}\Im_1-\left(1-2e^{-2i\phi}-e^{-4i\phi}\right)A_2-4e^{-4i\phi}E_4$$

$$d_3 = \frac{1}{6}\left[\left(\sin 4\phi - 2e^{-4i\phi} + 2e^{-6i\phi}\right)I_3 + \frac{1}{2}e^{-4i\phi}\Im_3 + \left(4e^{-2i\phi} - e^{-4i\phi} - 4e^{-4i\phi} - e^{-6i\phi}\right)\right]A_4 - 4e^{-6i\phi}E_6$$

$$d_2 = \frac{1}{8}\left[1 - \cos 4\phi + 8\sin^2\phi + 5i\sin\phi\left(e^{-5i\phi} - 2e^{-i\phi}\right)\right]\Im_1 + \frac{1}{2}\left(\cos 4\phi - 5i\sin\phi\, e^{-5i\phi}\right)I_3 + \Im_{3/4} + 2e^{-i\phi}E_6 +$$

$$+\left[i\sin\phi\left(3e^{-i\phi} - 2e^{-i\phi}\right) - e^{-2i\phi}\right] + \frac{1}{2}\left[2i\left(3e^{i\phi} - 3e^{-i\phi} - 2e^{-i\phi} + e^{3i\phi}\right)\sin\phi + e^{2i\phi} - 2e^{-2i\phi} - 16\sin^2\phi\, e^{-4i\phi}\right]E_4$$

$$\Im_n = 4\int_0^\infty y^{n+2} sh2y e(y)dy; \quad I_n = \int_0^\infty y^n[(1 - e^{-2y})sh2y - 4y^2]e(y)dy$$

$$A_n = \int_0^\infty y^n(ch2y - 1)e(y)dy;$$

$$E_n = \int_0^\infty y^n e(y)dy\,; e(y) = \frac{1}{4y^2 - sh^2 2y}$$

$$N_{11} = \frac{\pi^2}{48}(\cos 2\phi \pm 3); \quad N_{31} = \frac{\pi^4}{256}(\cos 4\phi/15 \pm \cos 2\phi); \quad N_{33} = \frac{N_{31}}{3}$$

Here and hereafter, the upper index corresponds to the right end of the defect, and the lower index to the left end.

Figures 2 and 3 show the relationships between $K_I^* = \lambda K_I/\sqrt{\pi l}Hql$ and $K_{II}^* = \lambda K_I/\sqrt{\pi l}Hql$ as a function of the crack rotation angle φ for $l/h = d = 0.1$ (Curves 1 and 2 correspond to the boundary conditions of the heat conduction problem: if the boundary temperature is specified as -1, or if the heat flux and heat transfer conditions are specified as 2), when the heat flux is perpendicular to the OY axis; solid lines correspond to the right end of the crack, dashed lines to the left; $H = \alpha t^{\circ}E/2$.

The figures show that the values of K_I and K_{II} in the absence of heat transfer (curves 2) are greater in absolute magnitude than when the boundary outside the contact zone is thermally insulated.

The value of K_{II} reaches its maximum when the heat flux is perpendicular to the crack.

The normal stress intensity factors K_I, which take on negative values, have no independent significance, since in this case it is necessary to solve the problem in a formulation that accounts for contact between the crack walls.

We investigate the stress intensity at the tips of a crack located at a depth of $\delta*$, when a temperature T_0 is maintained at its edges, and a heat flux $q(T, y)$ directed perpendicular ($\beta = 0$ —the angle between the flux direction and the Ox axis) to this surface is applied at the part's surface ($x = 0$). The thermoelastic state

of the machined surface will be determined solely by the disturbed temperature field. Given that along the line of a crack-like defect $T0 = 2q0 * \delta *$ from equations (17) – (19) and (21), we find:

$$K_I^{*\pm} = \mp q_0^* Hl\sqrt{\pi l}; \quad K_{II}^{*\pm} = \pm 2HT_0\sqrt{\frac{l}{\pi}} \tag{22}$$

If we introduce the quantity $P\eta = q0 * Hl\delta *$, where P is the tensile stress formed under the action of temperatures, andh is a parameter, then the following important characteristics for the behavior of defects can be established. If the values of the stress intensity factors are known, then the initial crack propagation angle $\theta *$ and the limiting value of the heat flux for it are determined from the relations [31], [32], [33]:

$$\theta_* = 2arctgD, \quad D = \frac{K_I - \sqrt{K_I^2 + 8K_{II}^2}}{4K_{II}} \tag{23}$$

$$q_{0*} = \frac{\sqrt{3}\lambda K_{1C}}{Hl\sqrt{\pi l}\delta^*} \tag{24}$$

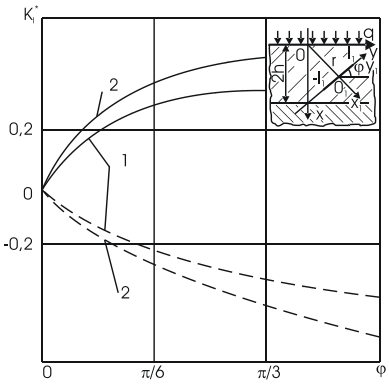

Fig. 2. Dependence of $K_I^* = \lambda K_I / \sqrt{\pi l} Hql = f(\phi)$ on the crack rotation angle φ at $\delta = l/h = 0.1$; 1 – when the boundary temperature is specified; 2 – when the heat flux and heat transfer conditions are specified; solid lines 1 and 2 represent the right end of the crack, and dashed lines represent the left end.

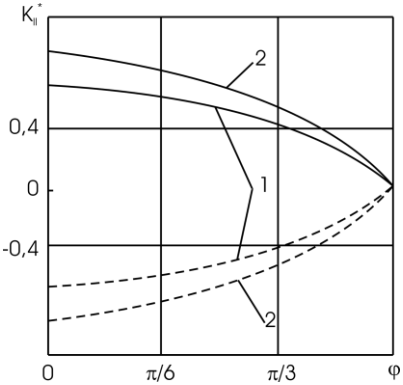

Fig. 3. Dependence of $K_{II}^* = \lambda K_I / \sqrt{\pi l} Hql = f(\phi)$ on the crack rotation angle φ at $\delta = l/h = 0.1$; 1 - Type I stress state; 2 - heat flux and heat transfer conditions are specified; solid lines 1, 2 - right, dashed lines - left ends of the crack.

Figs. 2 and 3 show the dependencies of the angle θ and the reduced tensile stress $\bar{P}_* = \sqrt{\pi l} \cdot P/K_{1C}$ at the right end of the crack on the angle α and various values of $\eta = q_0^* H l^*/p$.

Under the action of the heat flux, the thermally insulated crack begins to grow from both ends simultaneously. As shown in Fig. 2, with an increase in the heat flux, the ultimate stresses decrease, i.e., a disturbance of equilibrium is possible in the region of the defect under consideration, and a microcrack forms.

Let us consider the mutual influence of defects on stress intensity using the example of two arbitrarily oriented inhomogeneities. We will choose the origin on one of the inhomogeneities, and the second can move arbitrarily relative to the first. From equations (21) – (24), with $l_K = l$, $a_{ij} = a$, $\varphi_1 = 0$, $\varphi_2 = \varphi$, and $\delta = l/d$, after calculations accurate to δ^7,the SIF expression for the upper crack takes the form:

$$K_I^{\pm} = \frac{1}{\sqrt{\pi l} H q l}[0{,}5\delta - 0{,}25\delta^3 + 0{,}207\delta^5 - 0{,}0371\delta^7] \qquad (25)$$

$$K_{II}^{\pm} = \frac{1}{\sqrt{\pi l} H q l}[1 - 0{,}25\delta^2 + 0{,}195\delta^4 - 0{,}1787\delta^8] \qquad (26)$$

Fig. 4 shows the dependence of the values of K_s ($S = I$ – solid line, $S = II$ – dashed line) on the dimensionless distance between cracks $\alpha = a/2l$, calculated numerically using equations (25) and (26). When $\delta < 0.5$, the presence of the second defect has little effect on the value of K_{II}, whereas the coefficient K_I still depends significantly on the distance between the cracks. Fig. 5–10 shows the dependence of SIF on the angle φ (the angle of rotation of the second crack relative to the first) for $\delta = 1/3$ ($a = 3l$) when $\psi = 0, \pi/6, \pi/3, \pi/2$ (the curves are labeled with numbers 1–4 for the moving crack and 1′–4′ for the stationary crack; solid lines correspond to SIF at the right vertices of the crack (K_j^+), dashed lines at the left vertices (K_j^-).

The figures show that, for certain crack configurations, the coefficient K_I at one end may be negative (this means that the crack edges come into contact in the vicinity of that end). In this case, the SIF values in the vicinity of the other end of the macrocrack remain practically unchanged and can be used to determine the critical force at which the crack reaches a state of limit equilibrium.

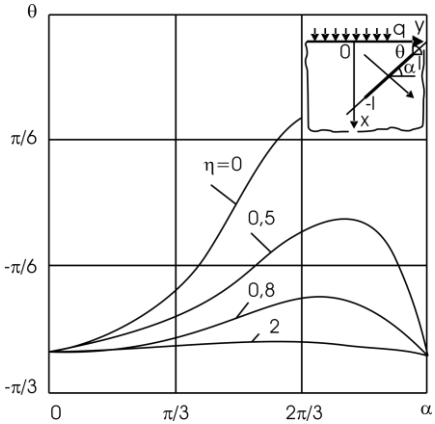

Fig. 4. Dependence of the initial crack propagation angle $\theta*$ on the angle α for various values of $\eta = q_0^* H l \delta^* / P$.

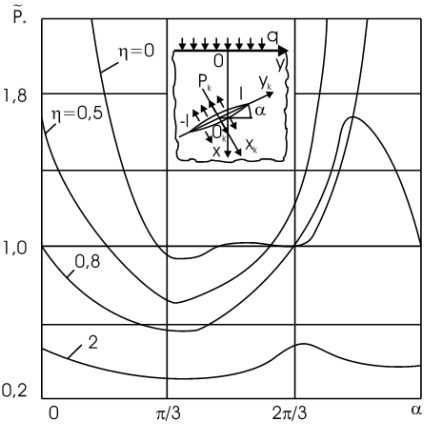

Fig. 5. Dependence of the reduced value of on tensile stresses $\tilde{P}_* = \sqrt{\pi l} \cdot P_* / K_{1C}$

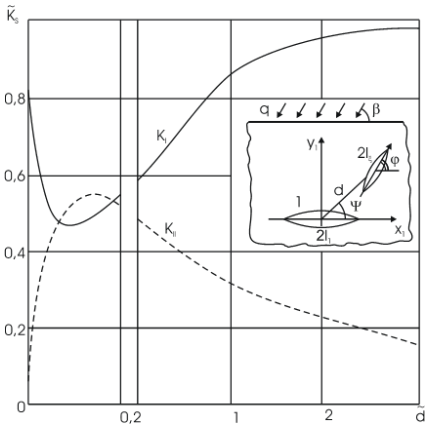

Fig. 6. Dependence of the value of K_s ($S = I$ – solid line, $S = II$ – dashed line) on the dimensionless crack spacing $\tilde{\alpha} = \alpha / 2l$.

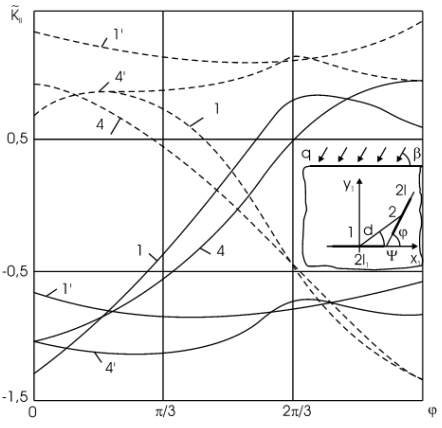

Fig. 7. Dependence of the value $\tilde{K}_{II}$ on the angle φ —the rotation of the second crack relative to the first—when $\delta = 1/3$, $\psi = 0$, $\psi = \pi/2$.

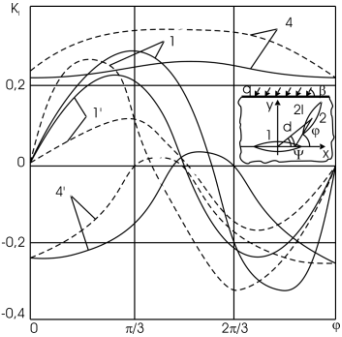

Fig. 8. Dependence of K_I on the angle φ of rotation of the second crack relative to the first at $\delta = 1/3$, when $\psi_1 = 0$, $\psi_4 = \pi/2$.

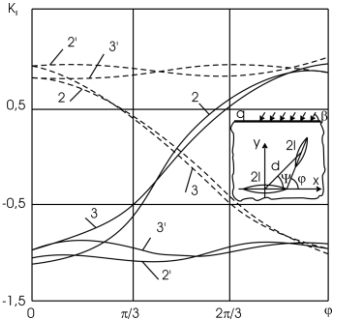

Fig. 9. Dependence of $K_{II} = f(\varphi)$ for $\delta = 1/3$, when $\psi_2 = \pi/6$, $\psi_3 = \pi/3$; solid lines—at the right vertices of the crack, dashed lines—at the left vertices.

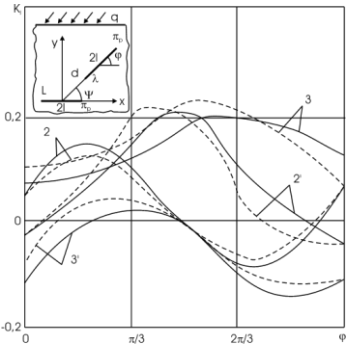

Fig. 10. Dependence of $K_I = f(\varphi)$ for $\delta = 1/3$ when $\psi_2 = \pi/6$, $\psi_3 = \pi/3$; solid lines—at the right vertices of the cracks, dashed lines—at the left vertices.

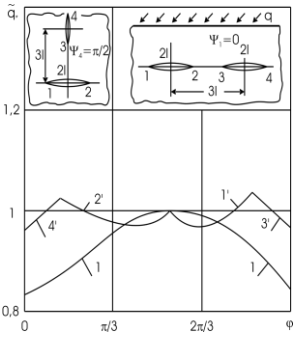

Fig. 11. Dependence of the critical heat flux value $\tilde{q}^* = q_0 l\sqrt{\pi l}/\sqrt{3}K_{1C}\lambda$ on the angle φ when $\delta = l/a = 1/3$.

For the values of SIF obtained from equations (7), (8), (17), and (19), the critical heat flux q^* is determined. The dependence of the reduced values $\tilde{q}^* = q^*/q_1$ ($q_1 = \sqrt{3}K_{1C}\lambda/(Hl\sqrt{\pi l})$ —corresponds to the value of the critical heat flux in a plane with a single crack) on the angle φ at $\delta = = l/a = 1/3$ is shown in Fig. 11. The curves labeled 1–4 correspond to the minimum value of $\tilde{q}^*$ at which crack propagation will begin from the corresponding vertex; the initial numbering of the crack vertices is chosen when $\varphi = 0$. Fig. 12 shows curves of the values $\tilde{q}^*$ for $\psi_1 = 0$ and $\psi_4 = \pi/2$ — for $\psi_2 = \pi/6$, $\psi_3 = \pi/3$ (the dashed curves correspond to the values $\psi_2 = \pi/2$ and $\psi_3 = \pi/3$).

It follows from the figures shown that when $0 \le \psi \le \pi/6$, a stationary crack begins to propagate first, and for all values of φ (with the exception of a certain region in the vicinity of $\varphi = \pi/2$) at vertex I. The critical heat flux has the smallest value for $\psi = 0$ and $\varphi = 0$ and for $\psi = \pi/6$ when $\varphi = \pi/2$. If $\psi = \pi/3$, then crack propagation begins from the bridge side, and the minimum value of $\tilde{q}^*$ is achieved when $\varphi = \pi/4$. In the case where $\pi/2 \le \varphi \le 5\pi/6$, the cracks mutually reinforce each other, i.e., the strength of the body in this case is higher than when there is only one crack. When $\psi = \pi/2$ and $\delta = 1/3$, the cracks practically do not interact.

Analysis of equations (16), which describe the thermally stressed state of the treated surface layer containing inclusions, allows us to determine the influence of the mechanical and thermophysical properties of these inclusions on the nature of their interaction with crack-like defects.

As an example, let us examine the stress state of a surface layer containing an inclusion with a crack (Fig. 13). We will present the solution to the heat conduction problem in the form:

$$T(S) = \frac{2q_0 l \sin\beta_0}{\lambda_{12}}\sqrt{1-S^2}\left[1 - \lambda_* \frac{\delta^2}{2} + \lambda_*^2 \frac{\delta^4}{4} - \lambda_* \left(S^2 + \lambda_*^2 + \frac{1}{2}\right)\frac{\delta^6}{8}\right] \qquad (27)$$

where $\lambda_{12} = \lambda_1 + \lambda_2$, $S = T/l$, $\delta = l/R$, $\lambda_* = \lambda_1/\lambda_2$. The stresses along the crack line are determined by the formulas:

$$\begin{aligned} -\sigma_x(S) &= -A_0 - 3A_1 S\cos\beta_0 \\ \tau_{xy}(S) &= -A_1 S \sin\beta_0 \end{aligned} \qquad (28)$$

where $A_0 = -\frac{4G_1(\alpha_2-\alpha_1)T_0}{2G+x_1-1}$; $A_0 = -\frac{2q_0 l G_1 \alpha_2 D_2^*}{\alpha_2(\hat{G}+x_1)}$; $D_2^* = \frac{2\lambda_2\alpha}{\lambda_{12}}$, a_1, a_2 are the linear thermal expansion coefficients of the insert and the matrix, respectively, $\tilde{\alpha} = a_1/a_2$

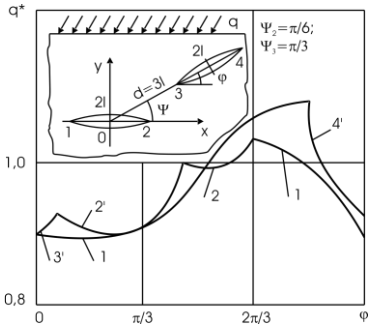

Fig. 12. Dependence of the critical heat flux value $\tilde{q}^* = q_0 l\sqrt{\pi l}/\sqrt{3}K_{1C}\lambda$ on the rotation angle φ of the crack-like defect of the second crack at $\delta = l/a = 1/3$.

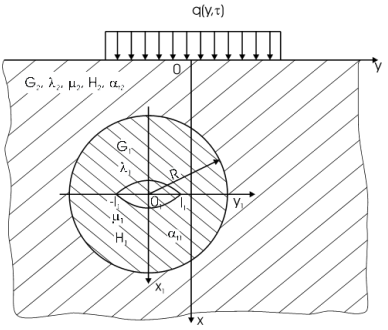

Fig. 13. Calculation scheme for determining the thermal stress state of a surface layer with an inclusion containing a crack-like defect.

G_1, G_2 - shear moduli of the inclusion and the matrix; $\tilde{G} = \mathrm{G}_1/\mathrm{G}_2$ - relative shear stiffness $H_{1(2)} = (3 - 4V_{1(2)})/(1 + V_{1(2)})$, $V_{1(2)}$ - Poisson's ratio of the inclusion (matrix): λ_1 , λ_2 - thermal conductivities of the inclusion and the matrix, respectively; q_o - heat flux acting on the boundary of the half-plane.

Substituting (28) into the formula:

$$K_j^{\pm} = C_j + \int_{-l}^{l} K_j^{\pm}(S)\sigma_x(S)dS \tag{29}$$

we find:

$$\begin{gathered} K_I^{\pm} = \sqrt{\pi l}\left[A_0\left(1 + \frac{1}{2}B_{10} + \frac{1}{8}B_{12} + \frac{1}{16}B_{14}\right) + \frac{3}{2}A_1 \cos\beta_0\left(\pm 1 + \frac{1}{4}B_{11} + \frac{1}{8}B_{13}\right)\right] \\ K_{II}^{\pm} = \sqrt{\pi l}\left[A_1 \sin\beta_0\left(\pm 1 + \frac{1}{4}B_{21} + \frac{1}{8}B_{23}\right) + \frac{q_0 H_1 \delta l}{\lambda_{12}}\sin\beta_0\left(\pm f_1 \pm 3f_2\frac{\delta^4}{4} + \frac{1}{4}f_1 B_{21}\right)\right] \pm \\ \pm \frac{H_1\sqrt{\pi l}}{4}\left[T_0 - \frac{l f_1 \lambda_*}{2\lambda_1}(2 - \lambda_*\delta^2)\frac{\delta^6}{32}\right]\left\{1 - B_1\frac{\delta^2}{2} + (9B_1 + C_1)\frac{\delta^4}{8} + (18 + 9B_1 + C_1)\frac{\delta^6}{32}\right\} \end{gathered} \tag{30}$$

where

$$B_1 = \frac{(x_1 + 1)}{(x_1 + \bar{G})}; \quad C_1 = -\frac{(x_1 + 1)}{(Gx_2 + 1)}$$

Analysis of the results shows that the presence of a hard switch ($V_1 > V_2$) leads to an increase in the value of K_I under mechanical loading and to a decrease under thermal loading. The thermal linear expansion coefficients of the composite have a significant influence on the nature of the change in SIF. For example, when $\alpha_{t1} < \alpha_{t2}$, $K_I > 0$, and when $\alpha_{t1} > \alpha_{t2}$, $K_I < 0$. The thermal conductivity coefficients λ_1 and λ_2 do not qualitatively affect K_I and K_{II}, but only alter them quantitatively. Thus, when $\tilde{\lambda} = 4$, the absolute value of SIF is greater than when $\tilde{\lambda} = 0.5$.

If the inclusion is considered as an ellipse, then when $\beta = 0$, the heat flux is directed parallel to the major axis; an increase in the stiffness of the inclusion ($V_1 > V_2$) according to the works [34], [35], [36], [37] leads to an increase in the stress intensity factors K_I ($K_{II} = 0$) for various composite $\tilde{\lambda}$.

The examples discussed above demonstrate the interaction between cracks and inclusions, as well as the stress state of a material containing these inhomogeneities. It has been shown that under certain conditions, stiffer inclusions strengthen the material, while softer structural components help inhibit the development of microcracks into main cracks. By appropriately selecting the material of the inclusions, the stress concentration in crack-like defects can be reduced.

Thus, for defect-free machining of workpieces made of functionally graded materials, their structural heterogeneity must be taken into account. The presence of crack-like defects and inclusions means that when selecting machining parameters and tool characteristics, one should be guided by the limiting values of the resulting heat flux.

To study the influence of the tool's design parameters on the part's temperature field, we will use the following discrete model. In the contact zone of length $2a$ between the wheel and the part, a heat flux $q(y,T)$ is formed due to the superposition of temperature pulses from individual grains of the wheel, equal to [38]:

$$q(y,\tau) = +\frac{C\sqrt{\tau_k}}{\lambda}[H(y) - H(y-2a)]\sum_{k=0}^{n}\delta\left(y + kl^* - V_{kp}\tau_k\right) \quad (31)$$

here $H(y)$ is the Heaviside function; $\delta(y)$ is the Dirac delta function; k is the number of grains passing through the contact zone during the time interval $\tau_k = \frac{\sqrt{D_{cr}t_{gr}}}{V_{cr}}$; a, λ are the thermal diffusivity and thermal conductivity of the workpiece material; $C\sqrt{\tau}$ is the heat flux from a single grain; V_g, V_{cr}, $\mathrm{t_{grind}}$ are the grinding conditions.

The fundamental solution to problems (2), (4), and (5) is known [39]:

$$G(x-x', y-y', \tau-\tau') = \frac{1}{4\pi a(\tau-\tau')}e^{-\frac{(x-x')^2+(y-y')^2}{4a(\tau-\tau')}}$$

Therefore, using Duamel's principle [40], the solution to problems (2), (4), and (5), taking (31) into account, can be expressed as:

$$T(x,y,\tau) = \frac{C}{2\pi\lambda}\int_0^{\tau}\frac{d\tau'}{\sqrt{\tau-\tau'}}\int_{-\infty}^{\infty}[H(y) - H(y-2a^*)]\,e^{\frac{2V_g y' + V_g^2\tau}{4a} + \frac{(y-y')^2+x^2}{4a(\tau-\tau')}}\sum_{k=1}^{n}\delta(y' + kl - V_{kp}\tau')\,dy'K_j^{\pm} = C_j + \int_{-l}^{l}K_j^{\pm}(S)\sigma_x(S)dS \quad (32)$$

or, moving to the desired function and applying the properties of the function $H(y)$, we obtain:

$$T(x,y,\tau) = \frac{C}{2\pi\lambda}\int_0^{\tau}\frac{d\tau'}{\sqrt{\tau-\tau'}}\int_0^{L}e^{-\frac{V_\partial(y-y')}{2a} - \frac{V_\partial{}^2(\tau-\tau')}{4a} - \frac{(y-y')^2+x^2}{4a(\tau-\tau')}}\sum_{k=0}^{\infty}\delta(y' + kl - V_{kp}\tau')\,dy' \quad (33)$$

This expression is already a solution to the problem, but it is inconvenient for practical calculations and research.

Using well-known transformations [41] and applying the properties of the delta function, we reduce the solution to a simpler form.

Due to the uniform convergence of the series under the integral, it can be integrated term by term, i.e.,

$$T(x,y,\tau) = \frac{C}{2\pi\lambda}\sum_{k=0}^{\infty}\int_0^{\tau}\frac{d\tau'}{\sqrt{\tau-\tau'}}\int_0^{L}e^{-\frac{V_\partial(y-y')}{2a} - \frac{V_\partial{}^2(\tau-\tau')}{4a} - \frac{(y-y')^2+x^2}{4a(\tau-\tau')}}\delta(y' + kl - V_{kp}\tau')dy' \quad (34)$$

Expression (34) can be simplified by using the definition of the delta function and the obvious inequality for the source coordinate y': $0 \le y' \le L = a*$; $K_l/V_{\text{кр}} \le \tau' \le (L+K_l)/V_{\text{кр}}$

$$\Im_k = \int_0^{L} exp\left[-\frac{V_\partial(y-y')}{2a} - \frac{V_\partial{}^2(\tau-\tau')}{4a} - \frac{(y-y')^2+x^2}{4a(\tau-\tau')}\right]\delta(y' + kl - V_{kp}\tau')dy' = \quad (35)$$

$$= exp\left[-\frac{V_\partial(y-y')}{2a} - \frac{{V_\partial}^2(\tau-\tau')}{4a} - \frac{(y-y')^2+x^2}{4a(\tau-\tau')}\right]$$

For $\tau' \overline{\in} \left[\frac{kl}{V_{kp}}; \frac{L+kl}{V_{kp}}\right]$, the integral $I_K = 0$. Applying the Heaviside function, this can be expressed as follows:

$$\Im_k = \left[H(\tau' - \frac{kl}{V_{kp}}) - H(\tau' - \frac{L+kl}{V_{kp}})\right] e^{-\frac{V_\partial(y+kl-V_{kp}\tau')}{2a} - \frac{{V_\partial}^2(\tau-\tau')}{4a} - \frac{(y+kl-V_{kp}\tau')^2+x^2}{4a(\tau-\tau')}}$$

The integral solution to (34) then takes the form:

$$T(x,y,\tau) = \frac{C}{2\pi\lambda}\sum_{k=0}^{\infty}\left[H(\tau' - \frac{kl}{V_{kp}}) - H(\tau' - \frac{L+kl}{V_{kp}})\right] exp\left[-\frac{V_\partial(y+kl-V_{kp}\tau')}{2a} - \frac{{V_\partial}^2(\tau-\tau')}{4a} - \frac{(y+kl-V_{kp}\tau')^2+x^2}{4a(\tau-\tau')}\right]\frac{d\tau'}{\sqrt{\tau-\tau'}} \quad (36)$$

This expression contains a Heaviside function under the integral. Using its properties, as before, we can determine the actual limits of integration. Solution (36) can be written in a form convenient for calculation:

$$\int_0^{\tau}\left[H(\tau' - \frac{kl}{V_{kp}}) - H(\tau' - \frac{L+kl}{V_{kp}})\right] f(\tau,\tau')d\tau' = H(\tau - \frac{kl}{V_{kp}}) - H(\tau - \frac{L+kl}{V_{kp}})\int_{\gamma_1}^{\gamma_2} f(\tau,\tau')d\tau' \quad (37)$$

where

$$\gamma_1 = \frac{kl}{V_{kp}}\left[H\left(\frac{kl}{V_{kp}}\right) - H\left(\frac{kl}{V_{kp}} - \tau\right)\right];$$

$$\gamma_2 = \frac{L+kl}{V_{kp}}H(\frac{L+kl}{V_{kp}}) - \left(\frac{L+kl}{V_{kp}} - \tau\right)H(\frac{kl}{V_{kp}} - \tau); \quad (38)$$

$$f(\tau,\tau') = exp\left[-\frac{V_\partial(y+kl-V_{kp}\tau')}{2a} - \frac{{V_\partial}^2(\tau-\tau')}{4a} - \frac{(y+kl-V_{kp}\tau')^2+x^2}{4a(\tau-\tau')}\right]\frac{1}{\sqrt{\tau-\tau'}}$$

And solution (36) takes the following form:

$$T(x,y,\tau) = \frac{C}{2\pi\lambda}\sum_{k=0}^{\infty} H(\tau - \frac{kl}{V_{kp}})H(\frac{L+kl}{V_{kp}})\int_{\gamma_1}^{\gamma_2} f(\tau,\tau')d\tau' \quad (39)$$

The initial conditions (4) imply that for all $K < 0$, expression (39) vanishes, and in fact the solution is constructed for $K \geq 0$.

The terms are the values of the function:

$$\Psi = \int_{\gamma_1}^{\gamma_2} e^{-\frac{V_\partial(y+kl-V_{kp}\tau')}{2a} - \frac{{V_\partial}^2(\tau-\tau')}{4a} - \frac{(y+kl-V_{kp}\tau')^2+x^2}{4a(\tau-\tau')}}\frac{d\tau'}{\sqrt{\tau-\tau'}} \quad (40)$$

This solution converges rapidly and thus reflects the actual grinding conditions. Indeed, the number of grains on the wheel passing along the contact arc at specific values of V_{kr} and V_g is limited. Therefore, the transition in expression (39) to a finite sum is justified, i.e., the temperature distribution of the part can be represented as:

$$T(x,y,\tau)=\frac{C}{2\pi\lambda}\sum_{k=0}^{\infty}H(\tau-\frac{kl}{V_{kp}})H(\frac{L+kl}{V_{kp}})\int_{\gamma_1}^{\gamma_2}f(\tau,\tau')d\tau' \quad (41)$$

Calculations in MathCAD for specific grinding conditions of magnetically hard alloys make it possible to trace the process of temperature field formation in the workpiece at the contact zone4 and study its kinetics.

The steady-state component of the temperature field, which does not depend on time, can be isolated from the general solution (41) as follows. Let us represent the intensity of the total heat flux as a time-periodic function with period $T = 2l$. We expand the delta function into a Fourier series over the interval $(-l/2V_{cr}; l/2V_{cr})$ [42]:

$$\delta\left(\tau-\frac{y}{V_{kp}}\right)=\frac{V_{kp}}{l}\sum_{-\infty}^{\infty}e^{ik\frac{\pi V_{kp}}{l}\left(\tau-\frac{y}{V_{kp}}\right)}$$

Taking this into account, the boundary condition (31) takes the following form:

$$\frac{\partial T}{\partial x}(0,y,\tau)=-\frac{C\sqrt{\tau}}{\lambda l}V_{kp}[H(y)-H(y-L)]\sum_{k=-\infty}^{\infty}e^{ik\frac{\pi V_{kp}}{l}\left(\tau-\frac{y}{V_{kp}}\right)}$$

The integral solution (3.2.3) in this case takes the form:

$$T(x,y,\tau)=\frac{CV_{kp}}{2\pi\lambda l}\int_0^{\tau}-\frac{d\tau'}{\sqrt{\tau-\tau'}}\int_0^{L}e^{-\frac{V_\partial(y-y')}{2a}-\frac{V_\partial{}^2(\tau-\tau')}{4a}-\frac{(y-y')^2+x^2}{4a(\tau-\tau')}}\sum_{k=0}^{\infty}exp\left[ik\frac{\pi V_{kp}}{l}\left(\tau'-\frac{y'}{V_{kp}}\right)\right]dy'$$

Let us make the following variable substitutions: $\tau-\tau'=Z;\ d\tau'=-dZt-t'=Z$ we obtain:

$$T(x,y,z)=\frac{CV_{kp}}{2\pi\lambda l}\int_0^{\infty}\frac{dz}{\sqrt{z}}\int_0^{L}e^{-\frac{V_\partial(y-y')}{2a}-\frac{V_\partial{}^2z}{4a}-\frac{(y-y')^2+x^2}{4az}}\sum_{k=0}^{\infty}exp\left[ik\frac{\pi V_{kp}}{l}\left(\tau-\frac{y'}{V_{kp}}-z\right)\right]dy' \quad (42)$$

If we set $K = 0$, then this expression does not depend on time and numerically characterizes the regular part of the part's temperature field:

$$T(x,y)=\frac{CV_{kp}}{2\pi\lambda l}\int_0^{\infty}\int_0^{L}e^{-\frac{V_\partial(y-y')}{2a}-\frac{V_\partial{}^2z}{4a}-\frac{(y-y')^2+x^2}{4az}}\frac{dz}{\sqrt{z}}dy' \quad (43)$$

Using the known relations [43], [44], we can rewrite (43) in a simpler form:

$$T(x,y,\tau)=\frac{CV_{kp}}{2\pi\lambda l\sqrt{V_g}}\int_0^{L}\sqrt[4]{(y-y')^2+x^2}e^{-\frac{V_\partial(y-y')}{2a}}K_{1/2}\left(\frac{V_\partial}{2a}\sqrt{(y-y')^2+x^2}\right)dy' \quad (44)$$

The impulsive component of the temperature field is expressed as:

$$T(x,y,\tau)=\frac{CV_{kp}}{2\pi\lambda l}\int_0^{\infty}\frac{dz}{\sqrt{z}}\int_0^{L}exp\left[-\frac{V_\partial(y-y')}{2a}-\frac{V_\partial{}^2z}{4a}-\frac{(y-y')^2+x^2}{4az}\right]\sum_{k=0}^{\infty}cos\frac{k\pi V_{kp}}{l}\left(\tau-\frac{y'}{V_{kp}}-z\right)dy' \quad (45)$$

On the surface (at $X = 0$), the expression for the steady-state component of the part's temperature field can be represented in terms of elementary functions. To

do this, we will use the well-known asymptotic representation of the Macdonald function for large values of the argument [45], [46]:

$$K_{1/2}(z) = \sqrt{\frac{\pi}{2z}} e^{-z} \tag{46}$$

Taking this into account, expression (44) takes the form:

$$T_k(0, y, \tau) = \frac{CV_{kp}a}{\lambda l V_g^2} \sqrt{\frac{\pi}{a}} \left\{ exp\left[\frac{(L-y)V_g}{a}\right] - exp\left[-\frac{V_g y}{a}\right] \right\} \tag{47}$$

In [45], [47], it is shown that when $U_{gl}/(2a) \geq 10$, the maximum of the temperature curve occurs at the point where the section of the machined surface exits the heating zone. In our case, this will be the point $y = L$. Then, considering that $L = \sqrt{Dt}$ [47], [48] from (3.2.18), we will have:

$$T_{kmax}(L, 0, \tau) = \frac{CV_{kp}a}{\lambda l V_g^2} \sqrt{\frac{\pi}{a}} \left[1 - exp\left(-\frac{V_\partial \sqrt{D_t}}{a} \right) \right]_{kmax} \tag{48}$$

The resulting expression (48) allows us to calculate the maximum contact temperature of the workpiece, which forms at the boundary between the contact zone and the zone of intense cooling, depending on the processing conditions, the characteristics of the grinding wheels used, and the thermophysical properties of the material being ground.

It is interesting to note that when calculating the maximum values of the steady-state component (T_K) and the instantaneous temperature of individual grains (T_M) for a specific material, and when experimentally evaluating the highest values of contact and instantaneous temperatures, a fairly good agreement between theoretical and experimental results was obtained.

The derived expressions for the instantaneous and contact grinding temperatures, as seen in equations (44) and (47), (48), depend on many technological parameters—grinding depth (t_{gr}), wheel speed (V_w) and workpiece speed (V_w), the grit size of the wheels used, the bond characteristics μ, the distance between cutting grains l and their number, as well as the thermophysical and mechanical properties of functionally graded materials.

In this regard, it appears possible to use these expressions as criteria for predicting the conditions under which defects such as burn marks form and the depth of their occurrence.

As for the study of the causes of grinding cracks, the micro-discontinuity of temperature fields, which is a consequence of the cutting process by individual grains, has a negligible effect on the nature and intensity of crack formation. The magnitude of the heat flux plays a greater role here.

Qualitatively new phenomena in the behavior of crack-like defects occur during macro-intermittent grinding, i.e., when wheels with an intermittent working surface are used [37], [49], [50].

Of interest is the behavior of the stress intensity factor K_I in the case of a non-stationary temperature field formed in the surface layer during grinding with intermittent wheels. To this end, let us consider the following problem.

In the contact zone $[-a*, a*]$, between the circle and the workpiece, there is a linear defect of length $2l$, part of which is located beneath the recess, while the remaining portion $2l - d$ is beneath the cutting edge. The heat conduction equation for this case takes the form:

$$a\left(\frac{\partial^2 T}{\partial x^2}+\frac{\partial^2 T}{\partial y^2}\right)=\frac{\partial T}{\partial \tau}-q\frac{(r)}{2\pi r}\delta(\tau), \quad r=\sqrt{(x-\xi)^2+(y-r)^2} \tag{49}$$

ξ, η — coordinates of the heat source; $\delta(r)$ —delta function. The boundary conditions will be, respectively,

$$\begin{aligned} &T(0,y,\tau)=T_k, \quad at \quad d<y<a, \tau>0 \\ &\frac{\partial T}{\partial x}(0,y,\tau)=T_k, \quad at \quad 0<y<d, \tau>0 \end{aligned} \tag{50}$$

The initial conditions coincide with (4).

The problem is solved using the Laplace integral transform [51] with respect to τ and the Hankel transform [47], [51] with respect to the variable r:

$$T_p(x,y)=\int_0^\infty T(x,y,\tau)e^{-p\tau}d\tau; \quad T_{p\alpha}(x)=\int_0^\infty T_p(r)\Im_0(\alpha r)\,dr$$

Performing the inverse Laplace transforms, we find

$$T_p(x,y,\tau)=\frac{q}{2\pi a}\int_0^\infty e^{-\alpha^2 a\tau}\alpha\,\Im_0(\alpha r)d\alpha=\frac{qe^{-\frac{r^2}{4a\tau}}}{2\pi a\tau} \tag{51}$$

We determine the thermal stresses by solving the Lamé equations (3) with boundary conditions (5).

We are interested in the case where an instantaneous heat source with intensity $q* = 1$ acts at the point $X = \xi_1 = 0$, $Y = \xi_2$. In this case, the solution takes the form:

$$\begin{aligned} \sigma_y(x,y,\tau)&=-\frac{\mu m}{\pi r^2}\left\{\left(1-e^{-\frac{r^2}{4a\tau}}\right)\left(1-\frac{2y^2}{r^2}\right)+\frac{(y-\xi)^2}{2a\tau}e^{-\frac{r^2}{4a\tau}}\right\} \\ \tilde{\sigma}_x(x,y,\tau)&=-\frac{\mu m}{\pi r^2}\left\{\left(1-e^{-\frac{r^2}{4a\tau}}\right)\left(1-\frac{2x^2}{r^2}\right)+\frac{x^2}{2a\tau}e^{-\frac{r^2}{4a\tau}}\right\} \\ \tilde{\tau}_{xy}(x,y,\tau)&=-\frac{r\mu m}{\pi r^2}(y-\xi)x\left\{\frac{e^{-\frac{r^2}{4a\tau}}}{4a\tau}-\frac{\left(1-e^{-\frac{r^2}{4a\tau}}\right)}{r^2}\right\} \end{aligned} \tag{52}$$

Using expressions (51)–(52), we can determine the temperature and stresses for heat sources $q(x,t)$ distributed along the axis $X = 0$, $Y > d$, with time-varying intensity. We previously established that the heat flux intensity is not

constant over time. Therefore, determining the thermal stresses for this case is of interest.

The temperature distribution in the part under these conditions will be:

$$T(x,y,\tau)=\int_0^{\infty}d\xi\int_0^{\tau}\left\{\frac{q(\varepsilon,\tau')}{4\pi a(\tau-\tau')}e^{-\frac{(y-d-\xi)^2+x^2}{4a(\tau-\tau')}}\right\}d\tau' \tag{53}$$

Then, the stress components can be found using the following formulas:

$$\begin{aligned}\sigma_y^{'}&=\int_0^{\infty}d\xi\int_0^{\tau}q(\varepsilon,\tau^{'})\bar{\sigma}_y(y-d-\xi,x,\tau-\tau^{'})d\tau^{'}\\ \sigma_x^{'}&=\int_0^{\infty}d\xi\int_0^{\tau}q(\varepsilon,\tau^{'})\bar{\sigma}_x(y-d-\xi,x,\tau-\tau^{'})d\tau^{'}\\ \tau_{xy}^{'}&=\int_0^{\infty}d\xi\int_0^{\tau}q(\varepsilon,\tau')\bar{\tau}_{xy}(y-d-\xi,x,\tau-\tau')d\tau'\end{aligned} \tag{54}$$

The stress state of the surface layer will not change if we replace the temperature function $T(x,y,\tau)$ with the expression $T(x,y,\tau)-TK$, since the stress components corresponding to uniform heating of the surface layer of the parts and vanishing at infinity are identically equal to zero. Therefore, equation (54) can be written as follows:

$$\sigma_x^{'}(0,y,\tau)=\mu xT_k+\mu x\int_0^1 T(0,y,\frac{\tau}{\alpha})d\alpha-2\mu xT(0,y,\tau) \tag{55}$$

Substituting the expression for the temperature distribution in item (53) into formula (55), we obtain the following expression for determining the stress state components on the surface $X=0$ in the form:

$$\begin{aligned}\sigma_x^{'}(0,y,\tau)\big|_{y<d}&=\mu xT_k+\frac{\mu xT_k}{\pi}\int_0^{\infty}\frac{1}{\tau^{'}\sqrt{\tau^{'}-1}}erfc\left[\frac{(d-y)\tau^{'}}{2\sqrt{a\tau^{'}}}\right]d\tau^{'}+\\ &+\frac{2}{\sqrt{\pi}}\frac{\sqrt{a\tau^{'}}}{(d-y)\tau^{'}}e^{-\frac{(d-y)^2\tau^{'2}}{4a\tau^{'}}}-\frac{2a\tau^{'}}{(d-y)^2\tau^{'2}}erf\left[\frac{(d-y)\tau^{'}}{2\sqrt{a\tau^{'}}}\right]\\ \sigma_x^{'}(0,y,\tau)\big|_{y>d}&=0\end{aligned} \tag{56}$$

To ensure that the edges of crack-like defects are stress-free at $y>0$, consider a stress state with components $\sigma_x^{''}$, $\sigma_y^{''}$, $\sigma_z^{''}$, chosen such that the following conditions are satisfied:

$$\tau_{xy}^{''}(0,y,\tau)=0;\quad \sigma_x^{'}(0,y,\tau)+\sigma^{'x} \tag{57}$$

For the normal stress $\sigma_x^{''}$ along the crack path, we obtain the expression:

$$\sigma_x^{''}(0,y,\tau)=\frac{1}{\pi\sqrt{|y|}}\int_0^{\infty}\frac{\sqrt{u}\sigma_x^{'}(o,u,\tau)}{u-y}du \tag{58}$$

Based on (53), (58), and (30), we find the stress intensity factor for the crack in the case of continuous contact, i.e., when the machined surface with a defect in the contact zone with the tool is subjected to continuous heating:

$$K = \lim_{y\to 0}\left[\sqrt{2\pi y}\sigma_x(0,y,\tau)\right] = 2\sqrt{\frac{2}{\pi}}\mu x T_k\sqrt{d} - \sqrt{\frac{2}{\pi}}\mu x T_k\sqrt{d}\frac{1}{\pi}\int_1^\infty \frac{d\tau'}{\sqrt{1-\xi}}\times$$
$$\times\left\{\int_0^1 erfc\left(\frac{\tau'}{\tau^*}\xi\right)\frac{d\xi}{\xi\sqrt{1-\xi}} + \frac{1}{\sqrt{\pi}}\frac{\tau'}{\tau^*}\int_0^1\left[e^{-\frac{\tau'^2\xi^2}{\tau^{*2}}} - \frac{\sqrt{\pi}}{2}\frac{\tau'}{\tau^*\xi}erf\left(\frac{\tau'}{\tau^*}\xi\right)\right]\frac{d\xi}{\xi\sqrt{1-\xi}}\right\} \quad (59)$$

here

$$\tau^* = \frac{2\sqrt{a\tau}}{d}, \quad \sigma_x(0,y,\tau) = \sigma'_x(0,y,\tau) + \sigma''_x(0,y,\tau)$$

Fig. 14 shows a graph of the dependence of the value.

$$K^* = \frac{K}{2\sqrt{2}\mu}\frac{\sqrt{\pi}}{xT_k\sqrt{a}}a\tau^*$$

As can be seen from the graph, the initial moments of time are the most dangerous in terms of crack propagation.

Consider the case where the surface layer with a defect at $X = 0, y > 0$ is subjected to a temperature field satisfying the following conditions on the $X = 0$ axis:

$$\begin{aligned} T(0,y,\tau) &= T_k, \quad at \quad d < y < d + l \\ T(0,y,\tau) &= 0, \quad at \quad y > d + l \\ \left.\frac{\partial T}{\partial x}\right|_{x=0} &= 0, \quad at \quad y < d \end{aligned} \quad (60)$$

In this case, the expression for the temperature on the $X = 0$ axis takes the form:

$$T(0,y,\tau) = \begin{cases} 1, & d < y < d + l \\ \frac{1}{\pi}\int_1^\infty\left\{erfc\left[\frac{|y-d|\tau']}{2\sqrt{a\tau}}\right] - erfc\left[\frac{|y-d-l|\tau']}{2\sqrt{a\tau}}\right]\right\}\frac{d\tau'}{\tau'\sqrt{\tau'-1}}, & y < d \end{cases} \quad (61)$$

For the stress intensity factor corresponding to this temperature field, we obtain the expression:

$$K = \sqrt{\frac{2}{\pi}}2\mu x T_k\sqrt{d}\left[1 - \sqrt{1+S} + F(\tau^*,S) - F(\tau^*,0)\right] \quad (62)$$

here

$$S = l/d, \quad F(\tau^*,S) = \frac{1}{2\pi}\int_1^\infty\left\{\int_0^1 erfc\left(\frac{\tau'}{\tau^*}(S+\xi)\right)\frac{d\xi}{\sqrt{1-\xi}} + \right.$$
$$\left.\frac{1}{\sqrt{\pi}}\frac{\tau_1^*}{\tau'}\int_0^1\left\{e^{-\frac{(S+\xi)^2\tau'^2}{\tau^{*2}}} - \frac{\sqrt{\pi}\tau^*}{2\tau'(S+\xi)}erf\left(\frac{\tau'}{\tau^*}(S+\xi)\right)\right\}\frac{d\xi}{(S+\xi)\sqrt{1-\xi}}\right\}\frac{d\tau'}{\tau'\sqrt{\tau'-1}}$$

The dependence of $K^* = \frac{K}{2\sqrt{2}\mu}\frac{\sqrt{\pi}}{xT_k\sqrt{a}}$ on τ^* is shown in Fig. 14.

The temperature field, in the case of intermittent contact between the tool and the workpiece with a crack-like defect in the machined layer (Fig. 15), leads to the emergence of compressive normal stresses along the defect, which helps to inhibit fracture propagation.

Thus, it appears possible to use local thermoelastic fields as a tool capable of controlling the trajectory and rate of defect propagation into cracks.

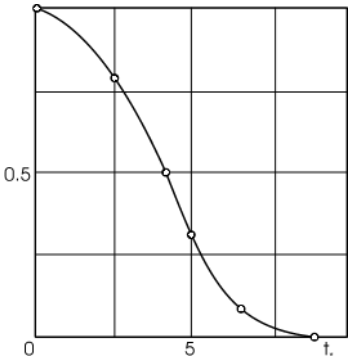

Fig. 14 Dependence of the stress intensity factor on time when the heat source is in full contact with the defect.

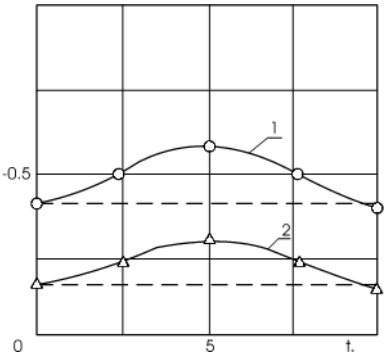

Fig. 15 Dependence of the stress intensity factor with time for intermittent contact between the heat source with the defect $1 - \lambda = 0.5; 2 - \lambda = 1 (l_{bc} = l_{bn})$.

The cutting depth t_{grind} is a determining factor in the formation of grinding cracks. The tensile transient stresses forming in the processing zone, which contribute to crack formation, are proportional to t_{grind}, since $T_K(O, y, \tau) \sim t_{grind}$.

$$\sigma_{\rho}^{max \frac{1+v}{1-v} t_k \left(\frac{x}{2\sqrt{a\tau}}\right)}$$

Therefore, when determining defect-free grinding parameters, it is necessary, first and foremost, to establish the maximum permissible cutting depths. In doing so, it is also important to have information not only on the thermophysical and mechanical properties of the material and the presence of inhomogeneities in the surface layer, but also on its processing conditions.

As heat transfer increases, high tensile stresses arise, contributing to the formation of grinding cracks on the machined surface.

Since the stress intensity factor for an isolated defect is determined by the formula [52], [53]:

$$K_1 = -\frac{1}{\sqrt{\pi l}} \int_{-l}^{l} \sigma_y(x, 0, \tau) \sqrt{\frac{l+x}{l-x}} dx$$

then, finally, p we obtain:

$$K_1 = \frac{GT_k(1+\nu)\alpha_t}{\sqrt{\pi l}}\left\{\pi l + \frac{2}{\pi}\int_{-l}^{l}\left[arctg\left(\frac{\sqrt{Dh}}{2(\xi+b)}\right) + arctg\left(\frac{\sqrt{Dh}}{2(b-\xi)}\right)\right]\sqrt{\frac{l+\xi}{l-\xi}}d\xi - \right.$$
$$\left. - \frac{1}{2\sqrt{\pi}}\int_{-l}^{l}\int_{0}^{\tau_k}\frac{1}{\tau\sqrt{a\tau}}\left[(\xi+b)e^{-\frac{(\xi+b)^2}{4a\tau}} + (b-\xi)e^{-\frac{(b-\xi)^2}{4a\tau}}\right]erf\left(\frac{\sqrt{Dh}}{4\sqrt{a\tau}}\right)\sqrt{\frac{l+\xi}{l-\xi}}d\tau d\xi\right\} \quad (63)$$

In the case where the stress intensity factor approaches the local failure criterion K_C in magnitude, the crack-like defect begins to develop into a crack. Thus, from the last relation, we obtain the equilibrium conditions for defects of length $2l$ in the form:

$$l_0 < \frac{K_C^2}{\pi[GT_k(1+\nu)\alpha_t]^2} \quad (64)$$

In this formula, the contact temperature T_K in the grinding zone depends on the process parameters and properties of the material being machined and can be determined by the formula:

$$T_k = \frac{CV_{kp}}{\lambda\sqrt{Dh}V_g^2}\sqrt{\frac{\pi}{a_n}}\left[1 - e^{-\frac{V_0\sqrt{Dh}}{a\tau}}\right]$$

where V_{cr}, V_g, h are machining conditions; D, C are tool parameters; λ, a_n — thermophysical characteristics of the workpiece material.

6. Conclusions

1. The values of the stress intensity factors for inherent inhomogeneities formed in the surface layer of products made of functionally graded materials are influenced by the size and orientation of these defects, their depth, their relative arrangement, and the magnitude of the heat flux during grinding.

2. For any values of the thermal conductivity, linear thermal expansion coefficient, and shear modulus of the material of the product and the inclusions located in the surface layer, when the stress intensity factors $K_I = 0$, $K_{II} \neq 0$ if the heat flux is directed perpendicular to the inhomogeneity within the inclusion, and conversely, if parallel to the crack, then $K_I \neq 0$, $K_{II} = 0$.

3. The geometry and properties of inclusions formed by previous operations in the surface layer can create conditions for both the inhibition and the propagation of grinding cracks. If the heat flux is directed parallel to the inclusion axis and a straight thermally isolated crack, then when the linear thermal expansion coefficient of the inclusion is greater than that of the matrix, the increase in the stiffness of the inclusion leads to an increase in the stress intensity factors K_I ($K_{II} = 0$) for various ratios of the thermal conductivity coefficients of the material components. This leads to the propagation of microcracks. Conversely, if the thermal expansion coefficient

of the inclusion is lower than that of the matrix material, a decrease in the stiffness of the inclusion leads to a decrease in the stress intensity factors K_I ($K_{II} = 0$) for the same ratios of thermal conductivity coefficients, i.e., conditions favorable for the non-propagation of microcracks are present.

4. For crack-like inhomogeneities located in a layer with a lower thermal conductivity coefficient a_t, the orientation of the microdefect strongly influences the value of SIF. When a microcrack located in a stiffer layer of the material being processed is significantly distant, the stress intensity factor K_I reaches its maximum values when the microdefect is oriented parallel to this line, and as the inhomogeneities approach, the maximum K_I is achieved when they are oriented perpendicular to the direction of the heat flux

5. The presence of a hard inclusion leads to an increase in K_I under mechanical loading and to a decrease under thermal loading. In this case, the thermal conductivity (TLCR) a_t has a significant influence on the nature of the stress intensity factor (SIF) variation. When the inclusion's $a_t < a_1$ of the matrix, $K_I > 0$, and when $\alpha_t^{incl} > \alpha_t^{(M)}$, $K_I < 0$. In a soft inclusion, a microcrack will begin to propagate at a lower heat flux than in a hard inclusion; that is, the strength of a body with a hard inclusion is higher than that with a soft inclusion

6. The micro-intermittent nature of the grinding process generates compressive stresses in the machined zone, which help reduce the incidence of grinding cracks. The stress intensity factor reaches its lowest values when the lengths of the cutting ridges and grooves of the intermittent grinding wheels are equal.

References: 1. A. A. Ferreira, 'Effects of Processing Parameters on Functionally Graded Materials for Industrial Components Repair', *MCMS*, vol. 4, no. 2, Sep. 2021, doi: 10.33552/MCMS.2021.04.000585. **2**. A. Usov, M. Kunitsyn, D. Klymenko, and V. Davydiuk, 'Modeling the effect of stochastic defects formed in products during machining on the loss of their functional dependencies', *Pratsi OPU*, vol. 1, no. 65, pp. 16–29, 2022, doi: 10.15276/opu.1.65.2022.02. **3.** F. Wöste, J. Kimm, J. A. Bergmann, W. Theisen, and P. Wiederkehr, 'Investigation of the effect of residual stresses in the subsurface on process forces for consecutive orthogonal cuts', *Production Engineering*, vol. 15, no. 6, pp. 873–883, Dec. 2021, doi: 10.1007/S11740-021-01058-Y. **4.** L. Jakubovičová, M. Vaško, and F. Synák, 'Evaluation of Load-Bearing Performance and Cost Efficiency in Steel-Welded and Modular Aluminum Rack Structures', *Machines*, vol. 13, no. 6, Jun. 2025, doi: 10.3390/MACHINES13060506. **5.** A. S. Kairov, V. Y. Oshovsky, and V. A. Kairov, 'INVESTIGATION OF THE EFFECT OF NANOCOATINGS ON THE WEAR-RESISTANCE OF SOCKET CARBIDE MILLS', Problems of computational mechanics and structural strength (in Ukrainian), no. 35, pp. 104–114, Dec. 2022, doi: 10.15421/4222220. **6**. V. Greshta, A. Yershov, V. Hrabovskyi, V. Vinichenko, and S. Seidametov, 'PHYSICAL-MECHANICAL CHARACTERISTICS AND THERMAL STRESS OF PLASMA COVERING', *New Materials and Technologies in Metallurgy and Mechanical Engineering*, no. 3, pp. 27–33, Oct. 2023, doi: 10.15588/1607-6885-2023-3-4. **7.** K. Osička, Z. Fišerová, J. Otoupalík, and J. Chladil, 'Tension of the Surface Layer in Machining Hardened Steels', *Manufacturing Technology*, vol. 17, no. 1, pp. 22–23, 2017, doi: 10.21062/UJEP/X.2017/A/1213-2489/MT/17/1/72. **8.** A. Salenko *et al.*, 'Forming a defective surface layer when cutting parts made from Carbon-carbon and carbon-polymeric composites', *Eastern-European Journal of Enterprise Technologies*, vol. 4, no. 1–94, pp. 61–72, 2018, doi: 10.15587/1729-

4061.2018.139556. **9.** G. Sun and Z. Ding, 'Effects of Heating Rate and Strain Rate on Phase Transformation in Micro-Grinding', *EPJ Web of Conferences*, vol. 224, pp. 05003–05003, 2019, doi: 10.1051/EPJCONF/201922405003. **10.** S. J. Eder *et al.*, 'Experimentally validated atomistic simulation of the effect of relevant grinding parameters on work piece topography, internal stresses, and microstructure', *Friction*, vol. 10, no. 4, pp. 608–629, Apr. 2022, doi: 10.1007/S40544-021-0523-3. **11.** A. Rajaei, B. Hallstedt, C. Broeckmann, S. Barth, D. Trauth, and T. Bergs, 'Numerical Prediction of the Microstructure and Stress Evolution During Surface Grinding of AISI 52100 (DIN 100Cr6)', *Integr Mater Manuf Innov*, vol. 7, no. 4, pp. 202–213, Dec. 2018, doi: 10.1007/s40192-018-0122-y. **12.** E. Sauter, E. Sarikaya, M. Winter, and K. Wegener, 'In-process detection of grinding burn using machine learning', *International Journal of Advanced Manufacturing Technology*, vol. 115, no. 7–8, pp. 2281–2297, Aug. 2021, doi: 10.1007/S00170-021-06896-9. **13.** I. Pavlenko *et al.*, 'Parameter identification of cutting forces in crankshaft grinding using artificial neural networks', *Materials*, vol. 13, no. 23, pp. 1–12, Dec. 2020, doi: 10.3390/MA13235357. **14.** P. Krajnik, K. Wegener, T. Bergs, and A. J. Shih, 'Advances in modeling of fixed-abrasive processes', *CIRP Annals*, vol. 73, no. 2, pp. 589–614, Jan. 2024, doi: 10.1016/J.CIRP.2024.05.001. **15.** R. Strunk, F. Borchers, B. Clausen, and C. Heinzel, 'Influence of subsequently applied mechanical and thermal loads on surfaces ground with mechanical main impact', *Materials*, vol. 14, no. 9, May 2021, doi: 10.3390/MA14092386. **16.** V. Stupnytskyy, E. Dragašius, S. Baskutis, and S. Xianning, 'Modeling and simulation of machined surface layer microgeometry parameters', *Ukrainian Journal of Mechanical Engineering and Materials Science*, vol. 8, no. 1, pp. 1–11, 2022, doi: 10.23939/UJMEMS2022.01.001. **17.** L. Urgoiti, D. Barrenetxea, J. A. Sánchez, and J. L. Lanzagorta, 'Detailed thermo-kinematic analysis of face grinding operations with straight wheels', *Metals*, vol. 10, no. 4, Apr. 2020, doi: 10.3390/MET10040524. **18.** A. A. Dyakonov and L. V. Shipulin, 'Geometric Model of the Interaction of the Grinding Wheel and Workpiece during Surface Grinding with the Periphery of a Straight Wheel', *Applied Mechanics and Materials*, vol. 756, pp. 41–46, Apr. 2015, doi: 10.4028/WWW.SCIENTIFIC.NET/AMM.756.41. **19.** W. Graham and A. T. Abdullahi, 'The nature of wheel-workpiece contact in surface grinding', *International Journal of Machine Tool Design and Research*, vol. 15, no. 3, pp. 153–160, 1975, doi: 10.1016/0020-7357(75)90017-7. **20.** C. F. Tiffany and J. N. Masters, 'APPLIED FRACTURE MECHANICS', *ASTM Special Technical Publication*, vol. STP 381, pp. 249–277, 1965, doi: 10.1520/STP26592S. **21.** G. I. Barenblatt, 'The Mathematical Theory of Equilibrium Cracks in Brittle Fracture', in *Advances in Applied Mechanics*, vol. 7, H. L. Dryden, Th. von Kármán, G. Kuerti, F. H. van den Dungen, and L. Howarth, Eds, Elsevier, 1962, pp. 55–129. doi: 10.1016/S0065-2156(08)70121-2. **22.** B. Skjetne and A. Hansen, 'Implications of realistic fracture criteria on crack morphology', *Frontiers in Physics*, vol. 7, no. APR, 2019, doi: 10.3389/FPHY.2019.00050. **23.** 'Fracture mechanics criteria and applications', *Choice Reviews Online*, vol. 29, no. 03, pp. 29–1536, Nov. 1991, doi: 10.5860/CHOICE.29-1536. **24.** P. Cornetti, N. Pugno, A. Carpinteri, and D. Taylor, 'Finite fracture mechanics: A coupled stress and energy failure criterion', *Engineering Fracture Mechanics*, vol. 73, no. 14, pp. 2021–2033, Sep. 2006, doi: 10.1016/J.ENGFRACMECH.2006.03.010. **25.** M. Kunitsyn, A. Usov, and Y. Zaychyk, 'The Influence of Cutting Forces on Cracks Formation During the Grinding of Products from Materials Prone to Defect Formation', in *Advances in Design, Simulation and Manufacturing VII*, V. Ivanov, J. Trojanowska, I. Pavlenko, E. Rauch, and J. Piteľ, Eds, in Lecture Notes in Mechanical Engineering. , Cham: Springer Nature Switzerland, 2024, pp. 240–250. doi: 10.1007/978-3-031-61797-3_20. **26.** Q. H. Qin, 'Trefftz finite element method and its applications', *Applied Mechanics Reviews*, vol. 58, no. 1–6, pp. 316–337, 2005, doi: 10.1115/1.1995716. **27.** F. L. de Silva Bussamra, E. L. Neto, and M. A. C. Rodrigues, 'Simulation of stress concentration problems in laminated plates by quasi-Trefftz finite element models', *Latin American Journal of Solids and Structures*, vol. 13, no. 9, pp. 1677–1694, 2016, doi: 10.1590/1679-78252698. **28.** A. Mioduchowski and Z. Płochocki, 'Thermal stresses in a coating layer. I. General theoretical scheme', *Acta Mech*, vol. 215, no. 1–4, pp. 319–333, Dec. 2010, doi: 10.1007/s00707-010-0345-2. **29.** W. T. Ang, 'A boundary integral equation for deformations of an elastic body with an arc crack', *Quarterly of Applied Mathematics*, vol. 45, no. 1, pp. 131–139, Apr. 1987, doi: 10.1090/QAM/885175. **30.** O. Maksymovych and A. Podhorecki, 'Determination of Stresses in

Composite Plates with Holes and Cracks Based on Singular Integral Equations', *Dynamical Systems Theory*, Mar. 2020, doi: 10.5772/INTECHOPEN.87718. **31.** P. S. Theocaris and G. A. Papadopoulos, 'Crack-propagation trajectories under biaxial loading, based on fracture criteria', *Journal of the Franklin Institute*, vol. 319, no. 4, pp. 443–456, 1985, doi: 10.1016/0016-0032(85)90013-4. **32.** D. Leguillon, E. Martin, O. Sevecek, and R. Bermejo, 'What is the tensile strength of a ceramic to be used in numerical models for predicting crack initiation?', *Int J Fract*, vol. 212, no. 1, pp. 89–103, Jul. 2018, doi: 10.1007/s10704-018-0294-7. **33.** H. F. Li, P. Zhang, B. Wang, and Z. F. Zhang, 'Predictive fatigue crack growth law of high-strength steels', *Journal of Materials Science & Technology*, vol. 100, pp. 46–50, Feb. 2022, doi: 10.1016/j.jmst.2021.04.042. **34.** F. Erdogan, 'Fracture problems in composite materials', *Engineering Fracture Mechanics*, vol. 4, no. 4, pp. 811–840, 1972, doi: 10.1016/0013-7944(72)90018-5. **35.** F. Erdogan, G. D. Gupta, and M. Ratwani, 'Interaction between a circular inclusion and an arbitrarily oriented crack', *Journal of Applied Mechanics, Transactions ASME*, vol. 41, no. 4, pp. 1007–1013, 1974, doi: 10.1115/1.3423424. **36.** H. Shen, P. Schiavone, C. Q. Ru, and A. Mioduchowski, 'Interfacial thermal stress analysis of an elliptic inclusion with a compliant interphase layer in plane elasticity', *International Journal of Solids and Structures*, vol. 38, no. 42–43, pp. 7587–7606, Sep. 2001, doi: 10.1016/S0020-7683(01)00033-6. **37.** J. Lee, S. Oh, and A. Mal, 'Calculation of interfacial stresses in composites containing elliptical inclusions of various types', *European Journal of Mechanics, A/Solids*, vol. 44, pp. 17–40, 2014, doi: 10.1016/J.EUROMECHSOL.2013.09.008. **38.** B. Gao, W. Bao, T. Jin, C. Chen, M. Qu, and A. Lu, 'Variation of wheel-work contact geometry and temperature responses: Thermal modeling of cup wheel grinding', *International Journal of Mechanical Sciences*, vol. 196, Apr. 2021, doi: 10.1016/J.IJMECSCI.2021.106305. **39.** V. N. Burlayenko, H. Altenbach, T. Sadowski, S. D. Dimitrova, and A. Bhaskar, 'Modelling functionally graded materials in heat transfer and thermal stress analysis by means of graded finite elements', *Applied Mathematical Modelling*, vol. 45, pp. 422–438, May 2017, doi: 10.1016/j.apm.2017.01.005. **40.** K. Topczewska and P. Zamojski, 'Effect of Pressure Fluctuations on the Temperature during Braking', *Acta Mechanica et Automatica*, vol. 14, no. 2, pp. 103–107, Jun. 2020, doi: 10.2478/AMA-2020-0015. **41.** P. Oza, K. Agarwal, and J. Tyagi, 'Fundamental solutions: a brief review', *Differential Equations & Applications*, no. 1, pp. 39–70, 2024, doi: 10.7153/DEA-2024-16-03. **42.** X. Xu, G. Li, Y. Zhao, and T. Liu, 'Analytical solutions for heat conduction problems with three kinds of periodic boundary conditions and their applications', *Applied Mathematics and Computation*, vol. 442, Apr. 2023, doi: 10.1016/J.AMC.2022.127735. **43.** A. A. Snarskii and I. V. Bezsudnov, 'Rotating thermoelectric device in periodic steady state', *Energy Conversion and Management*, vol. 94, pp. 103–111, 2015, doi: 10.1016/J.ENCONMAN.2015.01.058. **44.** M. Bayram, T. Partal, and G. Orucova Buyukoz, 'Numerical methods for simulation of stochastic differential equations', *Adv Differ Equ*, vol. 2018, no. 1, p. 17, Dec. 2018, doi: 10.1186/s13662-018-1466-5. **45.** S. C. Gupta, 'Temperature and moving boundary in two-phase freezing due to an axisymmetric cold spot', *Quarterly of Applied Mathematics*, vol. 45, no. 2, pp. 205–222, Jul. 1987, doi: 10.1090/QAM/895094. **46.** J. J. Shu and K. K. Shastri, 'Basic Properties of Incomplete Macdonald Function with Applications', *Journal of Function Spaces*, vol. 2020, 2020, doi: 10.1155/2020/6548298. **47.** J. L. González-Santander, 'Analytic solution for maximum temperature during cut in and cut out in surface dry grinding', *Applied Mathematical Modelling*, vol. 40, no. 3, pp. 2356–2367, Feb. 2016, doi: 10.1016/J.APM.2015.09.031. **48.** C. Salame and A. Malakizadi, 'An enhanced semi-analytical estimation of tool-chip interface temperature in metal cutting', *Journal of Manufacturing Processes*, vol. 105, pp. 407–430, Nov. 2023, doi: 10.1016/J.JMAPRO.2023.09.015. **49.** G. Anlas, M. H. Santare, and J. Lambros, 'Numerical Calculation of Stress Intensity Factors in Functionally Graded Materials', *International Journal of Fracture*, vol. 104, no. 2, pp. 131–143, Jul. 2000, doi: 10.1023/A:1007652711735. **50.** A. Fesenko, F. Yevsiukova, and O. Naboka, 'Development of a tool module for external intermittent grinding with the activation of the cutting fluid', *Mechanics and Advanced Technologies*, vol. 5, no. 2, Dec. 2021, doi: 10.20535/2521-1943.2021.5.2.234543. **51.** J. Pérez *et al.*, 'Heat transfer analysis of intermittent grinding processes', *International Journal of Heat and Mass Transfer*, vol. 51, no. 15–16, pp. 4132–4138, Jul. 2008, doi: 10.1016/J.IJHEATMASSTRANSFER.2007.11.043. **52.** E. Asadi, S. Fariborz, and M. Ayatollahi, 'Analysis of multiple axisymmetric annular cracks', *Journal of Mechanics of Materials and Structures*,

vol. 4, no. 1, pp. 1–11, Jan. 2009, doi: 10.2140/JOMMS.2009.4.1. **53.** J. Tweed, S. C. Das, D. P. Rooke, and D. P. Rooke, 'The stress intensity factors of a radial crack in a finite elastic disc', *International Journal of Engineering Science*, vol. 10, no. 3, pp. 323–335, 1972, doi: 10.1016/0020-7225(72)90047-X.

Анатолій Усов, Максим Куніцин, Юлія Сікіраш, Валерій Давидюк
Одеса, Україна,

ВПЛИВ МЕХАНІЧНИХ ТА ГЕОМЕТРИЧНИХ ХАРАКТЕРИСТИК НЕОДНОРІДНИХ ДІЛЯНОК НА ІНТЕНСИВНІСТЬ УТВОРЕННЯ ТРІЩИН ПІД ЧАС ШЛІФУВАННЯ ДЕТАЛЕЙ, ВИГОТОВЛЕНИХ ІЗ МАТЕРІАЛІВ З ФУНКЦІОНАЛЬНИМ ГРАДІЄНТОМ

Анотація. *Відсутність досліджень щодо особливостей виникнення шліфувальних тріщин та їх переростання в основні тріщини залежно від конструктивних, технологічних та структурних неоднорідностей матеріалу виробів не дозволяє однозначно застосовувати існуючі рекомендації щодо усунення зазначених дефектів. Ця робота присвячена дослідженню впливу внутрішніх неоднорідностей у поверхневому шарі, їх геометрії, та механічних характеристик виробів з функціонально-градієнтних матеріалів на вибір технологічних умов для бездефектної обробки деталей. Встановлено, що на величину коефіцієнтів інтенсивності напружень для внутрішніх неоднорідностей, що утворюються в поверхневому шарі виробів з функціонально-градієнтних матеріалів, впливають розмір і орієнтація цих дефектів, глибина їхнього залягання та взаємне розташування, а також величина теплового потоку під час шліфування. Геометрія та властивості включень, що утворилися в результаті попередніх операцій у поверхневому шарі, можуть створювати умови як для гальмування, так і для розвитку шліфувальних тріщин. Якщо тепловий потік спрямований паралельно осі включення і утворюється пряма, термічно ізольована тріщина, то коли коефіцієнт лінійного теплового розширення включення більший за коефіцієнт матриці, збільшення жорсткості включення призводить до збільшення коефіцієнтів інтенсивності напружень K_I ($K_{II} = 0$) для різних співвідношень коефіцієнтів теплопровідності компонентів матеріалу. Це призводить до поширення мікротріщин. І навпаки, якщо коефіцієнт теплового розширення включення нижчий за коефіцієнт матриці, то зменшення жорсткості включення призводить до зменшення коефіцієнтів інтенсивності напружень K_I ($K_{II} = 0$) при тих самих співвідношеннях коефіцієнтів теплопровідності, тобто створюються умови, сприятливі для нерозповсюдження мікротріщин. Тому при визначенні параметрів шліфування без дефектів необхідно, перш за все, встановити максимально допустимі глибини різання. При цьому важливо мати інформацію не тільки про теплофізичні та механічні властивості матеріалу та наявність неоднорідностей у поверхневому шарі, а й про умови його обробки.*

Ключові слова*: матеріали з функціональним градієнтом; неоднорідності; шліфування; утворення тріщин.*